

LOCALISATION OF MOBILE ROBOTS IN CHALLENGING ENVIRONMENTS

A THESIS SUBMITTED TO THE UNIVERSITY OF MANCHESTER
FOR THE DEGREE OF MASTER OF PHILOSOPHY
IN THE FACULTY OF SCIENCE AND ENGINEERING

2020

Yasin Alhamwy

School of Electrical and Electronic Engineering

Contents

Abstract	9
Declaration	10
Copyright	11
Acknowledgements	12
1 Introduction	13
1.1 Aims and Objectives	15
1.2 AVEXIS™	16
1.3 Research Outcomes	16
1.4 Thesis Structure	18
2 Literature Review	19
2.1 Underwater Localisation Methods	19
2.1.1 Odometry Based Localisation Systems	19
2.1.2 Absolute Positioning Systems	20
2.1.3 Simultaneous Localisation and Mapping (SLAM)	24
2.1.4 Discussion	25
2.2 Tether Localisation	27
2.2.1 Tethered Simultaneous Localisation and Mapping (TSLAM)	28
2.2.2 Indoor UAV Localisation Using a Tether	29
2.2.3 Smart Tether	29
2.2.4 3D Shape and Position Sensing Using Fibre Optics	30
2.2.5 Discussion	32
2.3 Summary	33

3	Tether Model	34
3.1	Background	34
3.1.1	Kinematics Model	34
3.1.2	Dynamics Model	35
3.1.3	3D Physics Engine-Based Simulation Environments	38
3.1.4	Discussion	38
3.2	2D Dynamics Model	40
3.2.1	Falling Tether	40
3.2.2	Tether Manoeuvred by Robot	45
3.3	Future Work	47
3.4	Summary	50
4	2D Tether Localisation System	51
4.1	Choosing a Sensor	51
4.1.1	Sensor Selection	52
4.1.2	Flex Sensor	53
4.2	Theory for the Tether Localisation System	57
4.3	Simulation and Experimental Results	60
4.3.1	Analysis of the Results From Each Method	65
4.3.2	Error Propagation From Sensor Measurements	67
4.3.3	Error Due to Sensor Separation Assumption	70
4.4	Challenges with proposed method	77
4.5	Summary	80
5	Camera Tether Localisation System	82
5.1	Challenges With Proposed System	85
5.2	Summary	86
6	Conclusion and Future Work	87
6.1	Future Work	88
A	Work done on the AVEXIS™	90
A.1	Variable Speed Control	90
A.2	Depth Hold	91
A.3	Thrust Allocation of Actuators	94

Bibliography

96

Word Count: 21594

List of Tables

2.1	Summary of the most common underwater localisation systems. . . .	26
2.2	Summary of tether localisation systems.	33
3.1	Summary of simulation methods for a long tether.	39

List of Figures

1.1	Picture of possible melted nuclear fuel inside the Fukushima nuclear plant [1].	14
1.2	Picture of the AVEXIS TM with a sonar attached below it in the Naraha Facility in Japan	17
2.1	The TSLAM problem [2].	28
2.2	Cross-Section of the fibre optic tether, where the smaller circles are the cores along the tether.	31
3.1	Picture of the AVEXIS TM with a sonar attached to it in the Naraha facility in Japan, with the tether behaviour shown. Marked are the dimensions of the AVEXIS TM and the approximate dimension of the tether loop.	37
3.2	A snapshot of the 2D falling elastic chain simulation.	40
3.3	Picture of the Vicon experiment for validating the 2D model. The silver balls attached to the tether are tracked via the Vicon system.	41
3.4	Simulated x position of each link at the defined time-steps.	42
3.5	x position from the Vicon system for each marker at certain time-steps.	42
3.6	Simulated y position of each link at the defined time-steps.	43
3.7	y position retrieved from the Vicon system for each marker at certain time-steps.	44
3.8	Snapshot of the simulation running as if the robot is moving the end point of the tether.	45
3.9	Simulated x position of each link at the defined time-steps.	46
3.10	Simulated y position of each link at the defined time-steps.	46
3.11	Picture of the cross-section of the tether attached to the AVEXIS TM	47
3.12	Picture illustrating the tensile test experiment.	48
4.1	Picture showing a sketch of the sensor nodes along the tether.	52

4.2	Picture of the flex sensor.	54
4.3	Picture illustrating how the flex sensor works [3].	54
4.4	Picture of the 3D printed test pieces.	55
4.5	Plot of measured angles when the flex sensor is held at 35.25°	56
4.6	Plot of measured angles from flex sensors when moved from a straight position to an angle of 79.3°	57
4.7	Picture illustrating the flex sensor approach.	58
4.8	Picture illustrating multiple flex sensor approach.	59
4.9	Points on grid to see if the model predicts the end point correctly.	61
4.10	Experiment rig with three flex sensors placed along the tether.	61
4.11	Picture illustrating multiple flex sensor approach with the sensor separation assumed to be a continuation of the arc of the circle.	62
4.12	Picture illustrating multiple flex sensor approach with the sensor separation assumed to be a continuation of the chord of the circle.	63
4.13	Picture illustrating the sensor separation as a continuation of the trajectory of the tip of the sensor.	64
4.14	Picture illustrating the sensor separation as an additional frame.	64
4.15	Estimated end position for each method when the end point is (15,20) cm.	65
4.16	Estimated end position for each method when the end point is (15,17) cm.	66
4.17	Error distribution for the x position estimations.	68
4.18	Error distribution for the y position estimations.	69
4.19	Log plot of the uncertainty in x position estimation of a 30 m Tether for varying sensor precision.	70
4.20	Picture illustrating the sensor separation error γ	71
4.21	Picture illustrating how γ affects the end position of a single sensor, where (x_{s0}, y_{s0}) is the end position of the sensor and (x_{p0}, y_{p0}) is the end position of the sensor including the sensor separation.	72
4.22	Plot of the error in the estimated x_{p0} position for varying γ values.	73
4.23	Plot of the error in the estimated y_{p0} position for varying γ values.	73
4.24	Picture illustrating the sensor separation error propagation, where the purple arrow approximately represents the uncertainty in the position of the end point of the sensor at different γ values.	74
4.25	Picture illustrating the γ propagation through the entire tether, assuming that γ will be present at all points.	75
4.26	Plot of the MSE in the x values for varying γ values.	76

4.27	Plot of the MSE in the y values for varying γ values.	76
4.28	Illustration of sensor node that houses the flex sensors.	78
5.1	Prototype for the camera node design	82
5.2	Illustration of the corner problem.	84
A.1	Test PCB designed for variable speed control	90
A.2	Image of the front side of the variable speed control PCB	91
A.3	Snapshot of AVEXIS TM from video showing its depth hold capabilities	92
A.4	Data from the AVEXIS TM while maintaining a depth of 20 cm. The data retrieved from the sensor was read to 4 significant figures.	92
A.5	Data from the AVEXIS TM while maintaining a depth of 20 cm. The data retrieved from the sensor was read to 2 significant figures.	93
A.6	Test rig deisgned to calibrate the pressure sensor to provide accurate depth readings	93
A.7	PWM to force allocation when the motor is ramping up from 0% duty cycle to 100%.	94
A.8	PWM to force allocation when the motor is ramping down from 100% duty cycle to 0%.	95

Abstract

The aim of this research is to investigate if tethered robots can be localised using sensors mounted along the tether, also known as tether localisation.

For environments where external infrastructure is not available for absolute positioning and conventional SLAM technologies do not work, tether localisation may be able to provide an estimation of position. An example of such an environment is the primary containment vessel (PCV) in reactor 1F at the Fukushima Daiichi Power Plant in Japan. Remotely Operated Vehicle (ROV) inspections are necessary to allow the safe decommissioning of the facility, however external beacons cannot be installed for absolute positioning and the water is too dark/turbid to allow for vision SLAM.

This thesis presents work conducted on tether localisation on a 2D plane. A simulation environment is implemented and experimentally validated using the Vicon systems. It was observed that the dynamic simulation of the tether provided some information about the tether's behaviour, however its accuracy is still unclear. Additionally, a kinematic simulation of the tether was implemented in order to see if it is viable to estimate the end location of a 0.30 m piece of tether using three low-cost commercially viable sensors.

The conclusion of this work is that the dynamic simulation of the tether requires much more work to provide a more realistic tether simulation as the current simulation does not consider the restoring forces of the tether. Additionally, the implemented short tether localisation system has many flaws and provided a varying error depending on the measured angle. The uncertainty of the sensor readings was $\pm 3.10^\circ$ which was implemented into the simulation to see the error propagation for a long tether. It was found that for a 30 m tether deployed along the y-axis on a 2D plane the average absolute error in the estimated position was (2.79,0.01) m, and the uncertainty in the estimated position was $\pm(3.00,9.68)$ m. These errors imply that expanding this system is unfeasible. It was discovered that in order to reach mm accuracy with 10 cm precision the sensor must provide measurements within $\pm 0.02^\circ$ of the actual value.

Declaration

No portion of the work referred to in this thesis has been submitted in support of an application for another degree or qualification of this or any other university or other institute of learning.

Copyright

- i. The author of this thesis (including any appendices and/or schedules to this thesis) owns certain copyright or related rights in it (the “Copyright”) and s/he has given The University of Manchester certain rights to use such Copyright, including for administrative purposes.
- ii. Copies of this thesis, either in full or in extracts and whether in hard or electronic copy, may be made **only** in accordance with the Copyright, Designs and Patents Act 1988 (as amended) and regulations issued under it or, where appropriate, in accordance with licensing agreements which the University has from time to time. This page must form part of any such copies made.
- iii. The ownership of certain Copyright, patents, designs, trade marks and other intellectual property (the “Intellectual Property”) and any reproductions of copyright works in the thesis, for example graphs and tables (“Reproductions”), which may be described in this thesis, may not be owned by the author and may be owned by third parties. Such Intellectual Property and Reproductions cannot and must not be made available for use without the prior written permission of the owner(s) of the relevant Intellectual Property and/or Reproductions.
- iv. Further information on the conditions under which disclosure, publication and commercialisation of this thesis, the Copyright and any Intellectual Property and/or Reproductions described in it may take place is available in the University IP Policy (see <http://documents.manchester.ac.uk/DocuInfo.aspx?DocID=487>), in any relevant Thesis restriction declarations deposited in the University Library, The University Library’s regulations (see <http://www.manchester.ac.uk/library/aboutus/regulations>) and in The University’s policy on presentation of Theses

Acknowledgements

Firstly, I would like to thank Simon, Joaquin and Andrew for their supervision. I am eternally grateful for everything that you have done for me and all the guidance that you have given me. I would also like to thank EPSRC for funding the project and allowing me to further my knowledge, skills and abilities. I would like to thank my family for always being there for me and I would also like to thank everyone in the robotics group for all their help and for all the fun time throughout the degree. Finally, I would like to thank Huda for all her support and for always being there for me.

Chapter 1

Introduction

Robots are very popular for underwater operations. The majority of these operations are conducted by Autonomous Underwater Vehicles (AUVs) and Remotely Operated Vehicles (ROVs). These vehicles are used to carry out numerous physical and sensing tasks in a wide array of applications. Specifically ROVs and AUVs have been used to aid in fossil fuel exploration, geophysical field surveys, salvage operations, offshore exploration [4, 5, 6, 7] and nuclear decommissioning inspection [8]. This means that the data can be collected from the environment without having any person exposed to the risks of the environment.

In the majority of these operations and tasks, the precise location of the robot is necessary for the robot's autonomous behaviour, accurate characterisation of the environment and the completion of the operation [7, 9, 10]. Traditionally, robots in outdoor environments such as drones or field robots use an absolute positioning system such as the Global Positioning System (GPS). However, for environments that are GPS denied robots will use simultaneous localization and mapping (SLAM) to localise themselves [11, 12, 13].

There are environments where neither absolute positioning systems or SLAM systems are suitable. The problem then arises with how does one localise a robot in these said environments? An example of one of these environments is the Fukushima Dai-ichi nuclear plant, where its reactors were damaged during an earthquake in 2011 and were stabilised by flooding them. The extent of the damage that was caused to the reactors is unknown. As part decommissioning process, ROVs were used to retrieve images (one shown in Figure 1.1) of the damage inside of the reactor [1]. The reactor

has a 150 mm access port which limits the size of robots and equipment that can be sent into the environment.



Figure 1.1: Picture of possible melted nuclear fuel inside the Fukushima nuclear plant [1].

The navigation of the ROVs was done via video feedback as no underwater localisation system currently exists that can function in these environments. There are many characteristics of the environment which make absolute positioning systems and SLAM systems unusable. GPS cannot be used for localisation as it uses radio waves that cannot penetrate through a body of water [5]. Other absolute localisation systems such as acoustic localisation systems are also unusable due to the multipath effects that occur in confined spaces and due to their complex calibration requirements [8, 14]. Additionally, electromagnetic (EM) systems are also unusable as they have very limited range before repeaters are required [15]. Furthermore, SLAM systems that use vision will not work due to the dark and turbid water and the lack of salient features [16]. Also SLAM that uses sonar systems struggles in enclosed environments [17]. This means that the only system that can be used in such environments are odometry based systems which are very inaccurate [18].

Another example of a challenging environment is Sellafield, which is also a GPS and SLAM denied environment. However, there have been multiple ROVs inside the Sellafield site but these ROVs lack positional knowledge which raises issues during manual operation (or requires highly skilled pilots). It does preclude the ability to use autonomy. Hence, the localisation of underwater vehicles is still the subject of a large amount of research [19, 20].

Therefore, a method to localise a robot in said environments is necessary in order for them to complete assigned tasks (such as autonomous surveillance). Due to the access constraints, the localisation system should not require any equipment to be added to the environment for it to work as it would be difficult to place and calibrate them in the environment.

Tethers are used for robots in nuclear environments for multiple reasons, such as: providing power to the robot and retrieval of the robot if it no longer functions, runs out of power or gets stuck in the environment [21, 22, 23]. Additionally, the tether provides a communication link enabling teleoperation of a robot in environments where wireless signals are insufficient or may not work [24].

Tethers can be problematic as they reduce the manoeuvrability of a robot [25], which causes a problem in unknown, potentially cluttered environments common in nuclear power plants such as Fukushima. The tether can get stuck on many obstacles and thus limit the robots movements. However, a tether is still considered a necessity in these types of environments due to the need to be able to retrieve the robot if it fails. Consequently, a localisation system that uses the tether is seen as preferable for AUVs and ROVs in these unknown, radioactive environments.

1.1 Aims and Objectives

The aim of this project is to investigate the feasibility of a tether localisation system for a robot. A tether localisation system is one that uses sensors mounted on the tether to estimate the position of the tethered robot. At first a 2-D plane solution in air would be investigated to see whether it is feasible to implement the system in 3-D, warranting further research. If the localisation system designed in this project is deemed unfeasible, this thesis will propose another method that may work.

The objectives for the project are:

- Understand the requirements for a model of a tether's kinematics.

- Implement a 2-D dynamic model for the tether to simulate its movements for different motions of the robot in order to figure out the effect of the tether on the robot.
- Investigate methods to measure the position of sensor nodes along the tether.
- Implement and analyse a proof-of-concept tether localisation system.

1.2 AVEXISTM

An example of an ROV which tether localisation could be implemented on is the AVEXISTM (Aqua Vehicle Explorer for In Situ Sensing (shown in Figure 1.2)), which is a small-scale underwater vehicle originally developed by the University of Manchester for the inspection of legacy nuclear fuel storage ponds at the Sellafield site in Cumbria [26]. The AVEXISTM has gone through three phases since the beginning of the project where it has been redesigned and reduced in size. The robot is designed to fit through the 150 mm access ports in both the Sellafield and Fukushima Daiichi sites. It is operated and powered via a tether which is also used to retrieve the video feedback from the camera on board the AVEXISTM. The robot can also carry an external radiation dose sensor and a short range sonar to help characterise the environment; however, these increase the overall size of the system and therefore it will not fit through the 150 mm access ports. Appendix A details work undertaken during this research on the AVEXISTM control systems.

1.3 Research Outcomes

This project focuses on in air localisation as it is easier to test and validate in comparison to underwater. The feasibility of tether localisation will be considered in air, and if deemed a practical solution, the implications of adapting the design to operate underwater will be considered.

This section outlines the outcomes of the project.

- **Tether model:** A pre-existing 2D dynamic elastic chain model was modified in order to simulate the tether's behaviour for different robotic manoeuvres.
- **Experimental validation of the proposed in air localisation system using low-cost, commercially available flex sensors:** A test rig was developed to

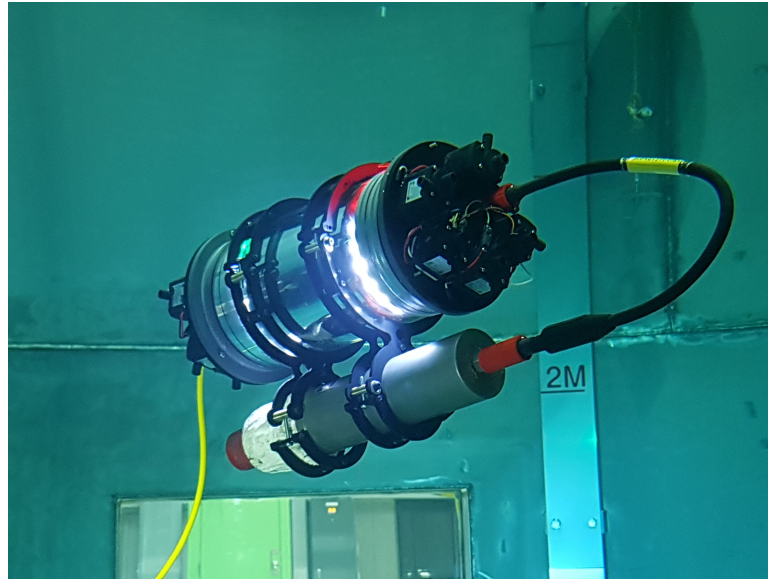


Figure 1.2: Picture of the AVEXIS™ with a sonar attached below it in the Naraha facility in Japan.

analyse the performance of the proof-of-concept system. The end point of the tether was calculated using a forward kinematic model and the results were analysed.

- **Analysis of sensor requirements:** An estimate for the required accuracy of the sensors was calculated. This estimate can be used to obtain accurate and precise localisation of the end point of the tether. A different localisation system (a visual system) was considered and discussed, however due to its many implementation challenges, it was concluded that Fibre Bragg Gratings (FBGs) may provide the best solution.

The contents of this thesis pertain to two localisation systems that fit the requirements outlined in Section 1.1. The feasibility of the first localisation system is investigated fully and the issues surrounding its application are discussed. The second localisation system is discussed briefly, however no judgements regarding its feasibility could be made due to the time constraints of the project.

1.4 Thesis Structure

This thesis is not presented in chronological order and a lot of the work was conducted concurrently. The thesis is outlined as follows; Chapter 2 focuses on the state of the art underwater localisation techniques and why they cannot be used in the target environments, the current state of the art tether localisation systems and why they cannot be used or why they are not suitable in the target environment. Chapter 3 focuses on the development and validation of a tether model. Chapter 4 investigates the proposed in air 2D plane localisation system and analyses the results obtained from it. Additionally, it discusses the weaknesses of the proposed system and why it should no longer be investigated and adapted into a 3D localisation system. Chapter 5 proposes another localisation system which is image based and it also discusses some of the strengths and weaknesses of said system if it were to be implemented. Finally, Chapter 6 concludes the thesis with a summary of the work achieved throughout the project and outlines any future work required.

Chapter 2

Literature Review

Chapter 1 outlined some of the challenges caused by specific nuclear decommissioning environments. Specifically, these environments are GPS and SLAM denied, which adds further problems to the existing challenges in underwater localisation.

This chapter will summarise the current underwater localisation systems and discuss their merits and feasibility for use in the Fukushima application described in Chapter 1. Furthermore, it would also review the current tether localisation systems and discuss their feasibility in the target environment.

2.1 Underwater Localisation Methods

Underwater localisation systems can be grouped into three categories; absolute positioning systems which require external infrastructure (GPS, acoustic, EM and visual), SLAM systems which use exteroceptive sensors and do not require external infrastructure (visual, laser and sonar) and odometry systems which generally use proprioceptive sensors and do not require any external infrastructure (visual and inertial navigation systems).

This section will discuss these systems and why they cannot be used in the target environment.

2.1.1 Odometry Based Localisation Systems

Odometry based localisation system uses the robot's motion and actuation systems to estimate the position of the robot. This can be done using three methods, inertial navigation systems [18], visual odometry [27, 28] or encoder-based odometry [28].

Visual Odometry:

Traditionally for wheeled robots, odometry is the process of calculating the position of the robot by measuring the wheel rotations, this estimation is imprecise due to the problem with the wheels slipping and sliding on the floor [28]. This method however, cannot be applied for robots with non standard locomotive methods such as underwater ROVs. Therefore, visual odometry is used instead, this determines equivalent information using camera images [27]. The reason why this system is impractical is due to the dark and turbid water in the environment and hence the estimation provided by this system will be very inaccurate or it will not work at all.

Inertial Navigation Systems (INS):

Inertial navigation systems (INS), are usually used as the core navigation system of robots due to their ability to continually provide measurements [18]. By using an inertial measurement unit (IMU) or other velocity and acceleration sensors the position of the robot can be calculated in the same way as odometry. The position of the robot for small time intervals can be accurate, however due to the inherent error accumulation, achieving accurate results over a long period of time using only an INS is impossible [18]. Furthermore, for really slow moving robots, such as the AVEXISTM, IMUs cannot pick up their acceleration as it is below the noise threshold [29].

To correct the drift and improve the navigation accuracy, these sensors are commonly paired with other sensors such as a Doppler velocity log (DVL), global positioning system (GPS) or an acoustic positioning system (APS) [30, 31]. The GPS position is not available underwater [30] and Doppler velocity logs are relatively large and cannot be deployed along side a robot that can fit through the 150mm access port in the mentioned environment. Therefore, other systems have to be considered and they have their respective downfalls in the target environment.

2.1.2 Absolute Positioning Systems

Absolute positioning systems require the installation of equipment inside or outside the environment in order for them to retrieve the absolute position of a robot [32, 33]. The most common absolute positioning systems are the global positioning system (GPS) [34, 35], acoustic positioning system [14, 33, 36], and electromagnetic positioning system [36, 37]. In some cases, image based systems are used to localise a robot

[15, 38]. As discussed previously, GPS cannot be used in the target environment as the radio signal cannot penetrate the body of water. Therefore, the other three systems need to be discussed and investigated.

Range Based Acoustic Positioning Systems:

Acoustic localisation systems are based on measuring the range between an acoustic modem (speaker) and a hydrophone (microphone designed to be used underwater) or vice versa and using the geometric relations between them [39].

There are three main categories of underwater acoustic positioning systems which are: long baseline (LBL), short baseline (SBL) and ultra-short baseline (USBL) or sometimes known as super-short baseline (SSBL) [14]. The baseline is the distance between the beacons within the calibrated network [40].

A LBL system has an array of transponders with a baseline of 50-2000+ m installed on the sea floor and obtains the range estimation to a responder mounted on an underwater vehicle [40]. The system then uses the range estimation between three or more transponders to estimate the position of the underwater vehicle [14]. Even though the system has very good positional accuracy independent of the water depth, this system is not usable in the target environment due to the required baseline. Additionally, the deployment of the transponders is expensive and time consuming and requires extensive calibration [14], which will be difficult if not impossible to do in the target environment. Furthermore, many radioactive environments will cause these transponders to fail after a sufficient dose [41, 42, 43]. This would further the expected cost and time consumption associated with this system as well as increasing the risk to manual operators.

A SBL system has a baseline between 20 and 50 m where the transponders are usually mounted on a surface vehicle/vessel and the responder will be mounted on the underwater vehicle. Since the system gives the position of the robot with respect to the transceivers mounted on the vessel, the system requires a Vertical Reference Unit (VRU), a gyro and in some cases a surface navigation system (such as the Global Positioning System (GPS)) to provide a position that is earth referenced [14]. This system can achieve high position accuracy without needing any transponders on the water environment's floor like the LBL system. However, the system requires transponders to

be placed with a baseline of 20 to 50 m on the water surface, which for the target environment might not be possible.

A USBL system has a baseline of less than 10 cm and consists of a transceiver, generally mounted on a pole and a single responder mounted on the ROV [44]. The system measures the phase comparison between them and uses the time of flight to calculate the distance (AoA) [14]. This system would be difficult to use in the target environment because it requires detailed calibration, it is very dependant on the VRU and is very susceptible to noise [45].

Range based acoustic localisation systems are the most common localisation techniques for underwater operations like oil and gas exploration. Which is mainly due to their ability of localising a robot up to 80/90 km away. Furthermore, it allows allows for two way communication with the robot for navigation and telemetry purposes [46], however this is not required for the target environment as the tether can be used for more reliable communication and a higher bandwidth.

Moreover, the performance of these systems in shallow water is poor and in enclosed environments the system can create strong multipath interference [8]. These environments can also have ambient noise which will also affect the performance. Additionally, other characteristics of the water like temperature gradients, salinity and turbidity can greatly affect the performance of the system [47]. Because of these limitations this system cannot be used in the proposed environment as it is an enclosed environment with unknown water characteristics and installing and calibrating the system is really difficult if not impossible. Hence other systems have to be considered to localise a robot in the target environment.

Electromagnetic (EM) Systems:

Electromagnetic (EM) signals can be used to localise an underwater robot [48]. Localisation systems that use EM signals use similar techniques to acoustic systems. This system exploits the fact that the power of EM waves attenuates rapidly with distance to estimate the distance to the source accurately when the output power is known [49]. Which is the same as the received signal strength indicator (RSSI) method in acoustic systems. The number of nodes required is dependent on the size of the environment. Hence, this is only practical for small environments.

The EM localisation system gives high accuracy (cm accuracy) of the position estimation [49]. However the main limitation of the system is its very short (<3 m) working range [37, 48] making it unusable in the target environment. Furthermore, the target environment (Fukushima) is filled with sea water which reduces the practicality of using EM systems due to the high attenuation of the signals in the environment.

External Image Based Localisation Systems:

Image based localisation systems work by retrieving the position and orientation of either an object in a camera image or resolving the position and orientation of the camera [50]. There exists two common methods to retrieve the position of the robot using image based localisation and they are external based image localisation systems and Visual Simultaneous Localisation and Mapping (V-SLAM), which will be discussed in Section 2.1.3.

An externally based image localisation system can be implemented with one or more cameras that have a line of sight of a robot equipped with a marker (e.g. LEDs, reflective targets, colours, etc.) and have a known reference point in the image [51]. The accuracy of the system depends on the quality of the image and the precision of the robot identification algorithm. An example of this system being used is its deployment in the Naraha test facility [15]. Where the designed system used an overhead camera with active markers mounted on the robot, environment markers and an on-board pressure sensor to measure the depth of the robot. These were used to transform the pixel position of the AVEXISTM into real world 3D coordinates [15].

This type of system provides high accuracy of the position estimation and lacks accumulated error [15]. However, this system requires continual, direct line of sight of the robot to estimate its position which limits the use of the technology in underwater environments that are cluttered or have high turbidity in the water. Despite that, this system can be implemented in a way which can avoid these limitations, as is further explained in Chapter 5.

2.1.3 Simultaneous Localisation and Mapping (SLAM)

A robot can build a map of the environment and simultaneously use this map to estimate its pose and position using a process called Simultaneous Localisation And Mapping (SLAM) [52]. This section will cover the SLAM systems that are used for underwater environments.

Visual Simultaneous Localisation and Mapping (V-SLAM):

If images are used to create the map, the SLAM process is called Visual-SLAM or V-SLAM. V-SLAM aims to estimate the camera trajectory while reconstructing the environment [53]. V-SLAM can be fused with INS systems (mainly IMUs) to increase the accuracy of the position estimation [54]. When building the map, V-SLAM identifies object landmarks in the environment and compares subsequent images with each other to estimate the position of the robot [55]. There are two types of V-SLAM; mono V-SLAM which uses one camera and stereo V-SLAM which uses two cameras instead of one (mono V-SLAM) to increase the accuracy [51].

The main issue with V-SLAM is that its range decreases drastically in muddy and turbid waters [50]. Additionally, it has difficulty in environments with too few landmarks to track [50]. This makes the use of V-SLAM difficult in the target environment described in Chapter 1 due to the dark and turbid water. Additionally, since this method requires large amounts of processing power, the operating time of an autonomous battery powered robot will be limited. However this last issue is not important for this project as any potential robot will be powered from a tether, and so will not be limited by its run-time.

Sonar Based Systems:

In water, acoustic signals can travel long distances without losing signal strength because sound waves can propagate through water. Sonars detect objects by transmitting and receiving signals (echoes) and are capable of detecting objects with a resolution of 20 mm and a range of 50 m [56]. The detected echoes from the environment can be used to reconstruct an acoustic image which can be used to implement SLAM algorithms [17].

The most common types of imaging sonar are the mechanically scanned imaging sonar, electronically scanned imaging sonar and the sidescan sonar [17]. The electronically

scanned imaging sonar is much more expensive than the latter.

Sonar systems can achieve highly accurate acoustic images in many underwater environments with many different characteristics (temperature, pressure, depth and visibility). However, in structured environments, feature extraction from the data requires significant post processing due to the noise in the sonar image which is caused by the production of ghost returns because of reflections [57, 58]. Therefore, this system struggles in enclosed featureless environments [59], meaning that this system is unusable in the target environment mentioned in Chapter 1. Another constraint of the mechanically scanned imaging sonar is that the robot is limited to very slow velocities because of the slow update rate [17]. However, for robots such as the AVEXISTM that will not be an issue due to its slow speed.

LiDARs:

LiDARs are generally used for performing SLAM in ground robots due to their high accuracy, latency and resolution [60]. However, because the laser can be attenuated and dispersed underwater, the use of LiDARs is limited in such environments. The current underwater LiDAR systems are generally used for general image 3D reconstruction of the environment due to its high resolution [61]. However, these underwater LiDARs are very large and hence can only be used on board large underwater vehicles. Therefore, this system is not applicable for this research as the target environment outlined in Chapter 1 necessitates a robot that can fit through a small access port.

2.1.4 Discussion

The target environment for this project is the Fukushima Daiichi nuclear plant, which has poor visibility with murky waters due to debris and sludge surrounding the pressure containment vessel (PCV). There are also a lot of mechanical structures in the water making it a confined and cluttered environment [15]. Therefore, creating multipath and shadowing effects which effects the accuracy and performance of acoustic systems. Furthermore, the cluttered environment will force the robot to be out of the field of view of external image based localisation systems which will stop the localisation system from functioning.

Additionally, the access to the target environment is limited to a 150 mm access

port [15] which limits the possibility of installing equipment that are required for the operation of acoustic and EM localisation systems. Moreover, sonar can work in the environment but it struggles in enclosed featureless environments due to reflections and ringing. The environment has dark and turbid water making visual localisation systems unusable. Therefore, none of the mentioned methods can localise a robot inside the target environment.

Table 2.1 shows a summary of the usability of the above mentioned systems in the target environment. The table highlights whether the system is able to operate without additional external infrastructure, whether the system is able to operate in SLAM denied environments (featureless with dark and turbid water) and finally if the system is usable in the target environment.

Table 2.1: Summary of the most common underwater localisation systems.

Technology	Acoustic	EM signals	Image	Odometry	Sonar	Lidar
Able to operate without additional external infrastructure?	No	No	method dependant	Yes	Yes	Yes
Abe to operate in SLAM denied environments?	Yes	Yes	No	Yes	depends on environment	No
Suitable for target environment?	No	No	No	No	No	No

The proposed localisation system that this project will focus on, will be using the tether of the robot. Using the tether would avoid the main unwanted environmental characteristics while also fitting the size constraint (to fit through access port). Therefore, it can be used to localise a robot in the Fukushima plant. In confined environments it might be the only viable method of localising the robot as it would not require any external equipment (such as beacons) to be added to the environment. This system once completed can be used for localising both underwater and ground robots.

2.2 Tether Localisation

The previous section has highlighted the fact that for an environment where additional external infrastructure cannot be used and where there is dark/turbid water, there is no suitable localisation technology. Localisation using sensors mounted on the tether is therefore an interesting topic to explore in further detail. This section will review the current state of the art tether localisation systems.

The localisation of the robot can be used for two different reasons. Firstly, it can be used so that an autonomous robot can calculate the required control action for it to complete its assigned task [62]. This implies that a precise estimation of the position is required so that the controller does not have to deal with sudden impulses in changes of the position. For example, the Jackal unmanned ground vehicle [63] and the DJI Phantom 4 RTK drone [64] use real-time kinematic (RTK) GPS to localise themselves, this localisation solution provides 1 cm accuracy with 0.01 cm precision. Since underwater robots which are much slower and experience much more damping compared to the two aforementioned robots, the precision and accuracy of the localisation system can be less than the RTK system while also providing a smooth control action.

Secondly, the localisation can be used to localise any target material (such as nuclear waste in Fukushima), in this case the precision of the localisation system has less effect on the control action of the robot however, it has an effect on the confidence of the estimated position of the target material. In this scenario the accuracy and the precision of the estimated position is what the user will be interested in. The international atomic energy agency (IAEA), which is an international organisation that seeks to promote the peaceful use of nuclear energy, specifies that the locations of nuclear material should be specific enough (within 1 m) to allow for prompt retrieval [65, 66]. Therefore a prospective tether localisation system must be able to provide the location to an accuracy of 1 m in the worst case scenario.

For example, nuclear waste is generally stored in 15,30 and 55 gallon drums [67, 68], the 55 gallon drum has a diameter of approximately 0.6 m and a length of 0.9 m. For such containers, as long as the estimated position is accurate, 1 m precision should provide high confidence in the position of the container. However, if the robot is required to localise smaller nuclear waste such as broken up fuel rods which consists of a number of pallets (which are 1 cm in diameter and 1 cm long) [69] the accuracy

and precision of the system needs to be much better. Therefore, the tether localisation system should localise the nuclear waste to approximately ± 10 cm.

2.2.1 Tethered Simultaneous Localisation and Mapping (TSLAM)

In cluttered environments the tether will get tangled around a number of ‘anchor points’ which complicates the navigation of the robot [2]. The University of Toronto has shown that by measuring the length of the deployed tether and the bearing to the most recent anchor points, they can formulate a TSLAM problem that allows them to estimate the pose of the robot and the position of the anchor points. When the robot moves in cluttered environments the tether would get tangled around obstacles and in order for it to return to the base station it must sequentially untangle itself from each obstacle. The system uses active anchor points (any obstacle currently in contact with a tether). By assuming that tether is always taut and knowing the length of the deployed tether, the bearing-to-anchor and the odometry of the robot it can estimate the position of the active anchors and the pose of the robot as seen in Figure 2.1.

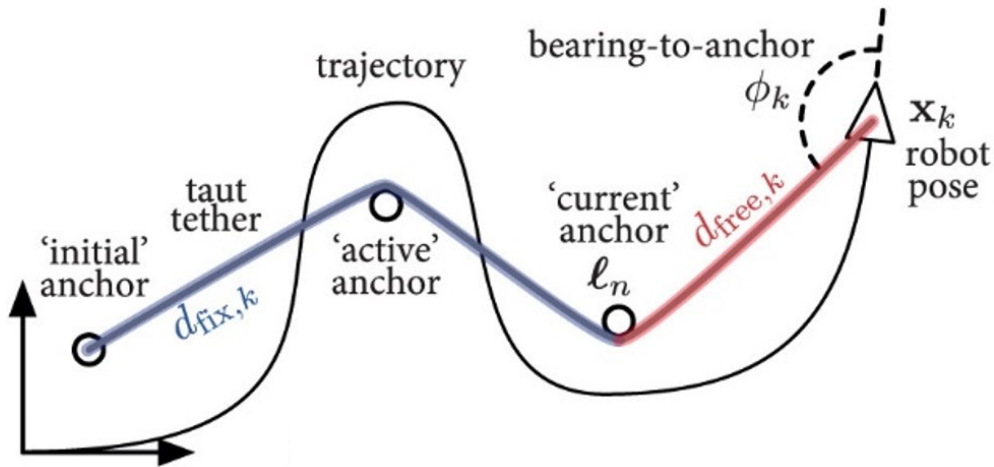


Figure 2.1: The TSLAM problem. Where the position of the anchor points and the pose of the robot are unknown and will be estimated by using the tether length, bearing-to-anchor angle, and odometry gathered along the trajectory [2].

This method could work in the proposed environment as it would work without having to place any external sensors in the environment. However, the system requires the odometry of the robot to be able to estimate the position of the robot. The odometry of underwater robotics can be obtained either by using IMUs (Inertial Measurement Unit) or visual odometry which uses stereo cameras. The problem with these two systems is that stereo cameras will not work in dark/turbid water and the IMUs accuracy

will decrease over time due to drift and it will also not work for slow moving underwater vehicles such as the AVEXISTM.

Additionally, as the system requires the cable to be taut at most times, this means the underwater robot must provide enough force to keep the buoyant tether taut which for a robot like the AVEXISTM is not possible or a smart tether spooling method has to be considered to release only the required amount of tether to keep the tether taut at all times. Furthermore, the accuracy of the system varies from 0.5 to 2 m depending on the length of the tether deployed and hence it is not accurate enough in cluttered environments.

2.2.2 Indoor UAV Localisation Using a Tether

Texas A&M University has designed an indoor UAV localisation system using a tether. The system uses the length of the tether, the tether azimuth and the elevation angle to estimate the position of the UAV by feeding the retrieved data into a mechanical model which retrieves an imaginary straight tether between the origin (centre of the tether reel) and the UAV [70]. The mathematical model works on the principle of the catenary curve, which is used to predict the geometric response of hanging cables under the effects of gravity [70].

This system works well in air as the cable will always be under the effects of gravity and this model would also work underwater if the tether was not neutrally buoyant. However, the majority of tethers used for underwater robots are neutrally buoyant to minimise its effects on the movement of the robot. Neutrally buoyant cables stay in their position underwater and therefore, this method of localising a tether cannot be considered as it will not work for the proposed application.

2.2.3 Smart Tether

KCF technologies have designed a smart tether which has sensor nodes embedded in the tether itself [71] and thus would not require any extra equipment to be installed in the environment. The sensor nodes are IMUs (Inertial Measurement Unit) that measure the acceleration, magnetic field and angular rate. The nodes are used to measure the orientation of the tether and use that information to estimate the position of the robot and the shape of the tether [71]. The system updates its position at 5 Hz and has an

accuracy of 1.5 m. This system can in theory be deployed in Fukushima; however, it is too inaccurate to provide a functional navigation system in a confined environment.

2.2.4 3D Shape and Position Sensing Using Fibre Optics

Multiple companies and universities have experimented with using fibre optics to measure the three dimensional shape or the location of an object.

Luna Innovations' position-sensing technology is based on Optical Frequency Domain Reflectometry (OFDR). OFDR allows for measuring the distributed strain along an optical fibre with high resolution, by using "phase-tracking techniques to compare Rayleigh scatter measurements with a baseline reference state" [72]. Luna Innovations experimented with a 30 m fibre optic cable which used Rayleigh scattering to determine the position of the end point. Rayleigh scattering (light scatter) that occurs in a core at specific axial locations of the optical fibre can be detected using Rayleigh scatter detectors. The accuracy of the measurement was approximately 1% of the length of the tether, at 0.2 Hz [72]. In one of the shape testing demonstrations, the RMS path measurement error was approximately 7.7 cm and a maximum measurement error of 13.5 cm was found. Where the path measurement error is the distance between a test point and the closest point on the 3D shape measurement [72].

The shape and position sensing is done through measurements of axial twist and curvature along the length of a helical multi core optical fibre. The distributed strain along the length of the centre core and the three outer cores (as seen in Figure 2.2) is monitored by OFDR techniques. The three outer cores are spaced at 120° from each other with respect to the centre of the core. This allows the shape-sensing fibre to convert the multicore distributed strain measurement into a 3D position [72]. When the tether bends, each of the outer cores experiences an alternating state of tension and compression along its helical path. Since the centre core is located in the centre of the sensing fibre it experiences very little first order strain while the other three cores exhibit sinusoidal strain responses that are 120° out of phase with each other. The amplitude and phase of the three strain curves can be compared to find out the bend radius and its direction relative to the fibre's coordinate system.

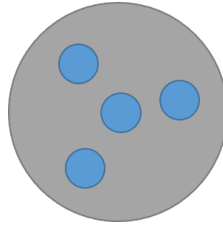


Figure 2.2: Cross-Section of the fibre optic tether, where the smaller circles are the cores along the tether.

Under twist, a common mode strain is experienced by the three outer cores. Depending on which way the tether is twisted, the three outer cores will experience either a tensile strain (if twisted in the direction of the helix) or compression (if the twist is in the opposite direction). The magnitude of the common mode strain signal allows the state of twist along the fibre to be determined. The centre core strain measurements are used to compensate for tensile strain and temperature changes in the fibre. The obtained twist measurement is used to convert the 3D curvature measurement relative to the tether's local coordinate system to a fixed 3D grid. The 3D grid is defined by the position and vector direction of the fixed start point of the fibre [72].

NASA have used low reflectance Fibre Bragg Gratings (FBG) and strain sensors in a multi-core fibre to provide much more accurate results in a 10 m tether, where NASA claims that their positional accuracy is (less than 1 mm) ten times better than any other comparable fibre based technique [73]. FBGs are used in multiple disciplines to sense different characteristics as they are sensitive to strain, temperature and pressure. FBGs can be attached (etched) or embedded into a fibre, this can be done via internal and external inscription techniques. In recent years, the external inscription techniques have become more prominent due to the inefficiency of the internal inscription techniques. Currently, three basic external inscription techniques exist: interferometric, phase mask and point-by-point inscription method [74]. FBGs work on the principle of blocking certain wavelengths of light that are transmitted along the core. NASA's approach relies on the characteristics of the FBGs. FBGs characteristics change depending on curvature and temperature, by sensing the relative change in three or more fibre cores an accurate change in 3D position can be determined. NASA also states their system provides high spatial resolutions for fibres up to 10 m long, the AVEXISTM currently uses a 50 m tether (which can be shortened) so a compromise in resolution and accuracy has to be made in order to increase the length of the fibre

core to the required length. In previous demonstrations of the AVEXISTMa maximum of 20 m of tether was actually deployed hence the tether can be cut down in length to 30 m for leeway.

The University of Twente researched using FBG sensors for closed loop control of flexible surgical equipment, demonstrating the use of an array of FBG sensors in a four-tendon driven manipulator to obtain strain measurements. These measurements were then used to reconstruct the 3D manipulator shape and this was used as feedback in a PID controller to steer the tip of the manipulator into the desired position. The system was demonstrated at high and low speeds for three different trajectory tracking cases, a circle (2D), a square (2D) and a helix (3D). They implemented an open loop and closed loop control and found out that the closed loop control greatly improved the performance of the system. The mean trajectory tracking errors of the open loop control were approximately ten times worse than the mean trajectory errors of the closed loop control. They also demonstrated the ability of the system to reject disturbances on the load by applying some weights to the tip of the manipulator, the system was still able to maintain the desired location despite the added load [75].

Current technology exist to measure the 3D shape and position along a fibre. This fibre can be attached with the tether of the robot. This technology seems to work quite well however it has a slow update rate. For example, the update rate of Luna innovations' solution gets slower as the length of the optic fibre increases (for a 1.5 m tether the update rate is 100's of Hz whereas for a 30 m tether it is 0.2 Hz [72]). Other localisation methods like the vision system designed by the University of Manchester [15] works at approximately 4 Hz and a typical 3D LiDAR like the velodyne vlp-16 works at a variable rate of 5-20 Hz [76]. Even though the proposed system is slower than the other mentioned localisation systems it is still an area of research.

2.2.5 Discussion

In conclusion, multiple methods for localising a tether exist. These methods all vary in terms of accuracy, speed and usability. Table 2.2 summarises the current tether localisation technologies that are being used. From Table 2.2 it can be seen that the only viable solutions to use in the cluttered unknown environment of the PCV in reactor

1F in the Fukushima Daiichi Power Plant in Japan are the FBG solutions. FBG solutions allow for very accurate localisation of the robot compared to the other methods; however, they are relatively slower than the other comparable systems. Another problem with FBG solutions is the length that can be used, NASA and Luna Innovations have claimed in their technical reports that they can locate the end point of a cable for lengths of 10 m and 30 m respectively; however, no implementation or publication was found validating their claims. Therefore, this project would consider other methods to localise the tether.

Table 2.2: Summary of tether localisation systems.

System Used	Smart Tether	Nasa's FBG approach	Luna's FBG approach	Indoor UAV localisation system	TSLAM
Technology used	Orientation based (IMUs)	FBGs	FBGs	Trivial sensors (encoders and IMUs)	Multiple sensors
Update Rate	5 Hz	Unknown	0.2 Hz	Unknown	Unknown
Accuracy	1.5 m	<1 mm	1% of Tether Length	0.3675 m	Varies with length
Length Tested	Unknown	10 m	30 m	Unknown	37 m
Implemented in real system?	Yes	Unknown	Unknown	Yes	Yes
Can it be used in suggested environment?	Yes, but highly inaccurate	Yes	Yes	No	No

2.3 Summary

In conclusion, there exists many underwater and tether localisation systems. The FBG solution is very promising however, due to the lack of publicly available information, and the high cost (£15,000+, dependant on the number of channels required), alternative solutions will be investigated. None of the other discussed solutions provide a viable solution to use in the target environment and therefore other methods and solutions need to be researched and developed.

Chapter 3

Tether Model

In order to estimate the position of the end point of the tether, the strain or the bend at specified points on the tether need to be measured, therefore sensors are required to be placed along the tether. The number of sensors required per meter will depend on the accuracy that is needed and it will also depend on how much the tether will bend for certain movements of the robot. Furthermore, the tether will have a force that will act on the robot which in return has an effect on the movements of the robot. Simulating the tether will allow for these movements and forces to be estimated. This section will explain the work done regarding the tether model.

3.1 Background

There are three possible methods for simulating the tether:

- Kinematics model.
- Dynamics model.
- 3D Physics Engine-based Simulation Environments.

3.1.1 Kinematics Model

The kinematics model studies the motion of bodies without considering the forces that cause the motion. Kinematic models are generally used to estimate the end position of manipulators with actuated joints using forward kinematics, or the joint angles required to place an end effector at a given location (inverse kinematics). If the tether is assumed to be a manipulator with a very large number of non-actuated links, forward

and inverse kinematics can be used to estimate the end position or the behaviour of the tether. Kinematic models are not as computationally demanding as the other modelling methods [77], therefore they can be used to provide real-time tether end position estimation, which will be discussed in Chapter 4.

Prior work at the University of Manchester has simulated a moving tether using multiple cylinders (straight links) connected by joints [78]. The length of the cylinders will depend on the flexibility of the tether; the more flexible it is the shorter the cylinders. In a similar manner, the section between sensors can be assumed to be straight links. The sensors provide information to allow for the transformations to be measured. This information can then be used to provide the homogeneous transformation matrices required to compute final position and orientation of the robot. The challenge with such an approach is defining the link lengths based on the mechanical properties of the tether, this is because the smallest errors in the definition can propagate throughout the system leading to a high uncertainty in the solution (which will be evident in Chapter 4).

Kinematic models cannot be used to accurately estimate the behaviour of the tether from the robot's movement as they do not account for the complex reactive forces that are dependent on a number of mechanical properties. Therefore, a dynamics model has to be used to provide accurate simulation of the tethers movements.

3.1.2 Dynamics Model

The dynamics model of a system studies the motion of bodies due to an applied force. Therefore, by knowing the force that a robot is applying, the behaviour of the tether can be simulated. To get an accurate estimation of the behaviour of the tether an understanding of the internal and external forces on the tether is required. This method is computationally inefficient as integration is required to determine the positions and velocities of each point at each time step. The computational inefficiency limits the applicability of using a dynamic model to provide real-time tether position estimation, however it would provide accurate simulation of the tether's behaviour for different robotic movements.

Developing a tether model that works in air on a 2D plane can be seen as an intermediate step to developing a tether model for use underwater. A 2D dynamic simulation was implemented by the University of Alabama which simulates the behaviour of an elastic chain with several point masses connected by elastic springs which can only support tension [79].

The 2D equation of motion for this model is the following:

$$F = F_{ext} - F_{damp} - F_{spring} \quad (3.1)$$

Where $F = \mathbf{M}\vec{u}$ is the force due to gravity on each particle (where \mathbf{M} is the mass matrix and \vec{u} is the acceleration vector), F_{ext} is the force manoeuvring the end point, $F_{damp} = \mathbf{C}\vec{v}$ is the viscous damping force on each particle (\mathbf{C} is the viscous damping coefficients matrix and \vec{v} is the velocity vector) and $F_{spring} = \mathbf{K}\vec{d}$ is the force generated from the elastic springs (\mathbf{K} is the spring constants matrix and \vec{d} is the displacement of each point mass). This equation of motion does not consider the internal damping of the tether.

This model will be explored, modified and experimentally validated in this Chapter.

Underwater Tether Models

The dynamic model mentioned above considers the tether to be in air, which is an important starting point to see if the model is behaving as expected. However, the target environment mentioned in Chapter 1 is an underwater environment and hence when designing a tether localisation system specifically for that environment, an underwater tether model is required.

The problem arises from the fact that the majority of tethered underwater robots use neutrally buoyant tethers as they have limited effect on the manoeuvrability of the robot (in terms of weighing the robot down). This means that the tether stays in its position underwater (can be seen in Figure 3.1) and does not tend towards a specific shape. Therefore, modelling it becomes a challenging task.

There is little research conducted in designing tether models for neutrally buoyant cables. The one approach that was found is the lumped mass approach which considers the tether to be a series of point masses connected together by massless, elastic

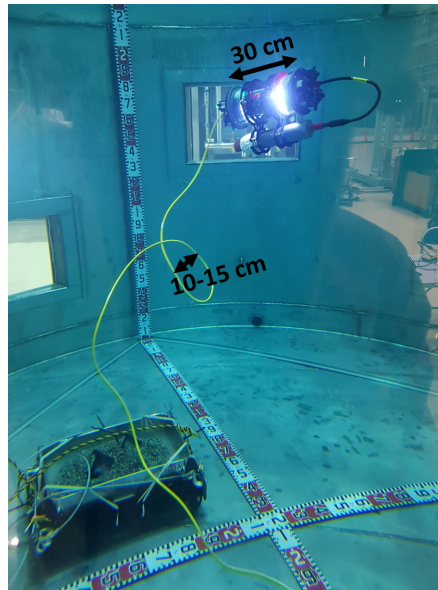


Figure 3.1: Picture of the AVEXISTM with a sonar attached to it in the Naraha facility in Japan, with the tether behaviour shown. Marked are the dimensions of the AVEXISTM and the approximate dimension of the tether loop.

springs. This approach is widely used to model tethers because it takes into account the bending effects, which are crucial for obtaining realistic results from low-tension manoeuvres [80].

The University of Victoria has designed a dynamic mathematical model for the towing cable of a submersible vehicle. Where the model considers the internal forces generated by the cable's elastic behaviour and the external forces generated by the surrounding environment such as hydrodynamic drag, weight and buoyancy [81, 82, 83]. For this model to work, the endpoints of the cable element need to be known so that the Euler angles can be calculated. Taking all of these forces into account and the internal forces of the tether, the equation of motion for an underwater neutrally buoyant cable becomes much more complicated [82]. This model should provide adequate results when a simulation of an underwater cable is required.

3.1.3 3D Physics Engine-Based Simulation Environments

Another option to simulate the behaviour of the tether is to use physics simulation packages, like Vortex Studio which is a real-time simulation and visualisation software [84]. This software has built in models to simulate neutrally buoyant cables, however as how they work is not explained, it was opted to start with a different solution so that an understanding of the tether's behaviour can be gained. An advantage of using such a software will be that a mathematical model will not be required, however the user must learn to use the program and create the required simulation. Furthermore, the software is expensive and computationally demanding.

3.1.4 Discussion

Using the three mentioned models to estimate the tether behaviour will have some differences. Firstly, the kinematic and dynamic models must be written in a programming language (like MATLAB) in order to simulate the forces, while on a physics simulation software the user would set up the simulation in terms of the components and the movements that make up the system, then with the provided information the software will compute the required forces. An advantage of implementing the model on to a software like MATLAB is that the user has much more control over what the simulation does. Additionally, the user can retrieve whatever information they like from the system, like the forces and positions of each section. Whereas on the simulation software, the user would be limited to what data the software provides to them.

When a real time simulation of the tether is required, a kinematics or a simulation software can be used to provide real time data, whereas a dynamics model cannot provide real-time data for long tether lengths. Finally, collisions and physical limitations are difficult to simulate and consider using kinematic and dynamic models, on the other hand a physics simulation software can account for these collisions and physical restraints to some extent. However, the accuracy of such a simulation is unknown. Table 3.1 provides a comparison between the mentioned methods to simulate a tether.

In conclusion, to simulate the behaviour of the tether for different robotic movements a dynamic model will be investigated to build an understanding of how a tether is expected to behave. Then 3D physics engine-based simulation environments will be considered. The kinematic model will be used for estimating the end position of the

Table 3.1: Summary of simulation methods for a long tether.

Method	Kinematics Model	Dynamics Model	Simulation Environments
Accurate Simulation of the tether's behaviour?	No	Yes	currently unknown
Can the end position be estimated?	Yes	Yes	Yes
Implementation difficulty	low	high	software dependant
Can it be run in real-time?	Yes	No	Yes
Does it account for collisions and physical limitations?	No	No	software dependant
Cost	low	low	high

tether localisation system due to its low computational requirements and its ability to run in real time.

3.2 2D Dynamics Model

Two simulations were developed, one of which was the tether falling due to gravity, i.e. F_{ext} was the force on the tether due to gravity. The second simulation was of the tether being manoeuvred by a robot, i.e. F_{ext} was the force applied by the robot. Both of these simulations use the model described in Section 3.1.2.

3.2.1 Falling Tether

The dynamics simulation code provided by the book *Advanced Mathematics and Mechanics* [79] was edited to pivot one point of the cable and allow the other end to free fall. Figure 3.2 shows a snapshot of the simulation in MATLAB where an approximate value of stiffness and viscous damping coefficient (\mathbf{K} and \mathbf{C} respectively in Equation 3.1) .

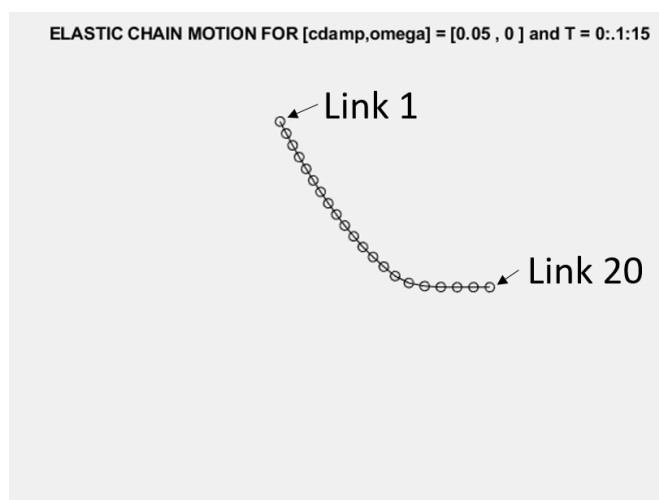


Figure 3.2: A snapshot of the 2D falling elastic chain simulation. The video of the simulation is available at: <https://youtu.be/jt4oaFG6z50>

In order to see if the model provides accurate movement of the tether, the simulation was run for a 1.45 m tether with 5 cm link lengths. The model takes the stiffness of each string and the viscous damping coefficient as physical parameters, however due to timing constraints, these values had to be estimated. Figures 3.4 and 3.6 show the x and y position of each link at each time-step. This provides some data which can be validated and compared to a real world experiment.

The validation is done by placing tracking balls on a robotic tether and having the Vicon system (which is a motion capture system that provides sub mm accurate

localisation of markers [85, 86]) track the movement of each ball and record that data. Figure 3.3 shows a picture of the tether hanging with the tracking markers attached at known intervals. A single marker represents one of the links in the simulation. During the experiment, an issue kept occurring with the last marker, where it no longer gets tracked after a few seconds. The experiment was repeated 10 times and this problem kept occurring. Therefore, that marker cannot be compared with the corresponding link. Additionally, the Vicon system record data in frames and to get a comparable plot to the simulation they were converted to time (the experiment had 6825 frames at 250 Hz). Figures 3.5 and 3.7 show the x and y position of each link at each time-step retrieved from the Vicon system.

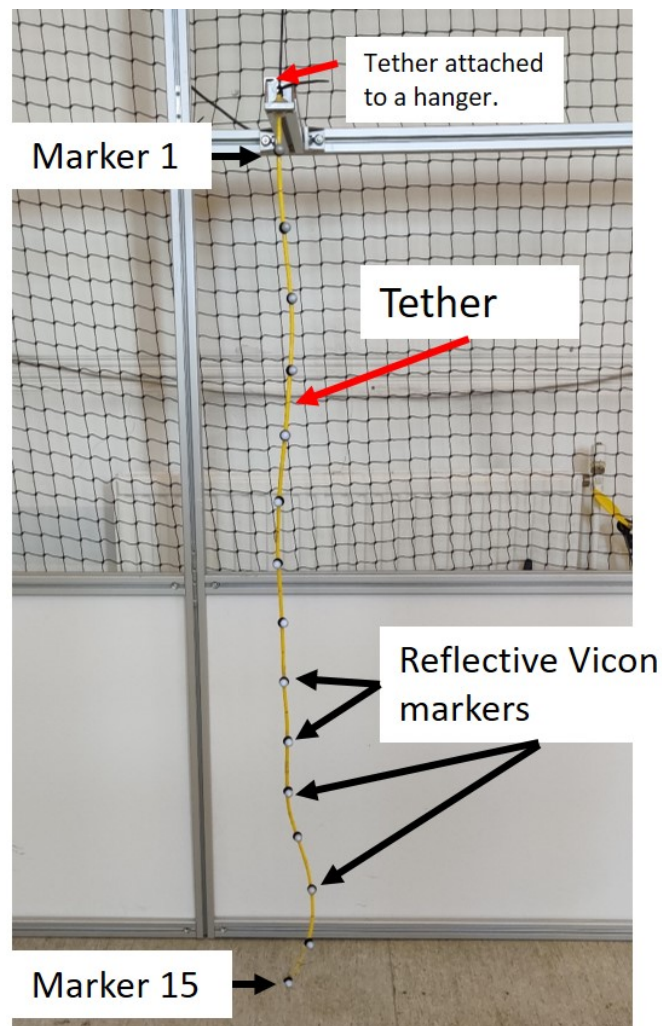


Figure 3.3: Picture of the Vicon experiment for validating the 2D model. The silver balls attached to the tether are tracked via the Vicon system.

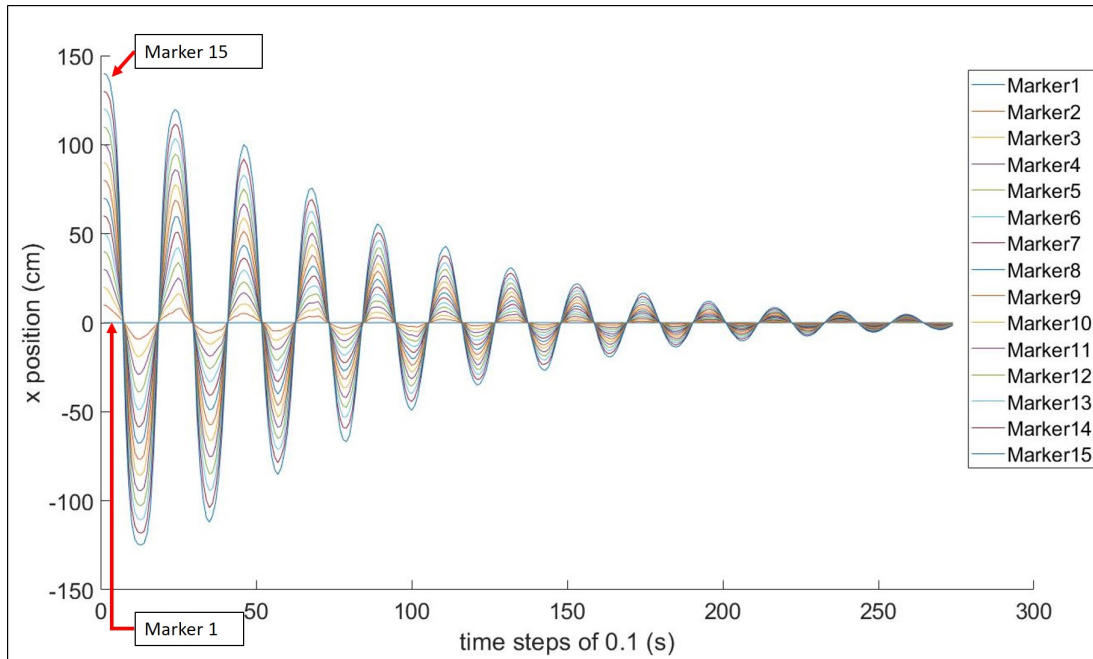


Figure 3.4: Simulated x position of each link at the defined time-steps.

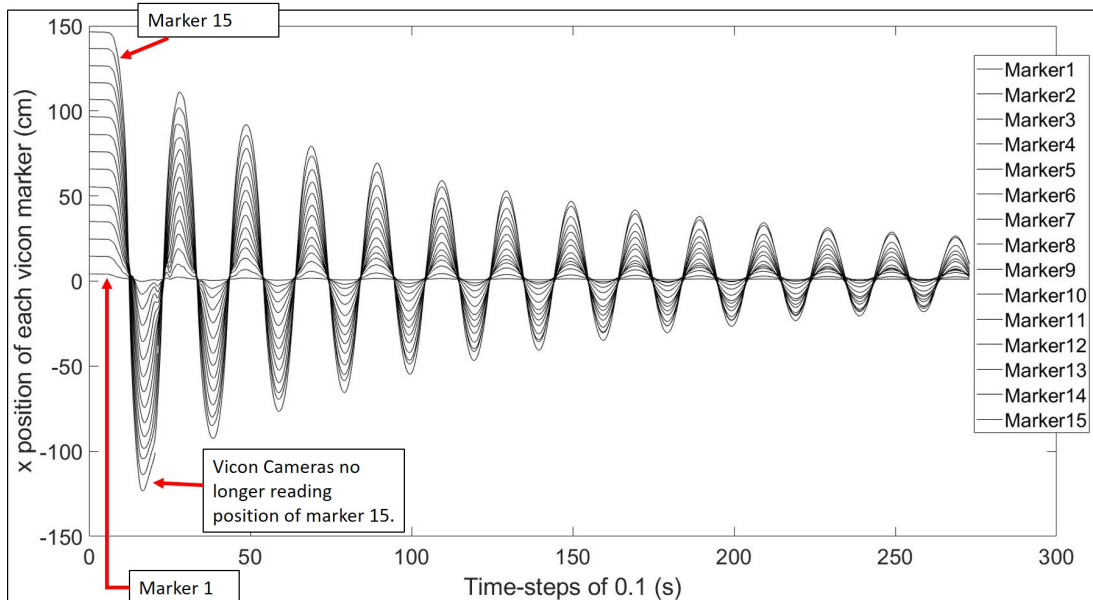


Figure 3.5: x position from the Vicon system for each marker at certain time-steps.

The simulated and experiment results provide comparable movements of the tether falling due to gravity. The first noticeable difference between the simulated and the experimental results is the greater damping in the simulation compared to the real-world experiment. At first, it is obvious that reducing the damping coefficient in the result should yield more comparable results however, reducing the damping coefficient (C in equation 3.1) further in the simulation causes issues with the links wrapping around each other. This is due to the fact that the model does not consider the restoring forces of the cable and does not also consider the angular forces of the tether. These forces will stop the tether from overlapping as it would naturally want to return to its original shape. Estimating the damping coefficient of the actual tether so the value can be input into the simulation model is difficult as it is actually a linear viscous damping coefficient proportional to each particles velocity. Each particle in the model is assumed to be infinitesimally small and hence, getting an accurate value would be difficult.

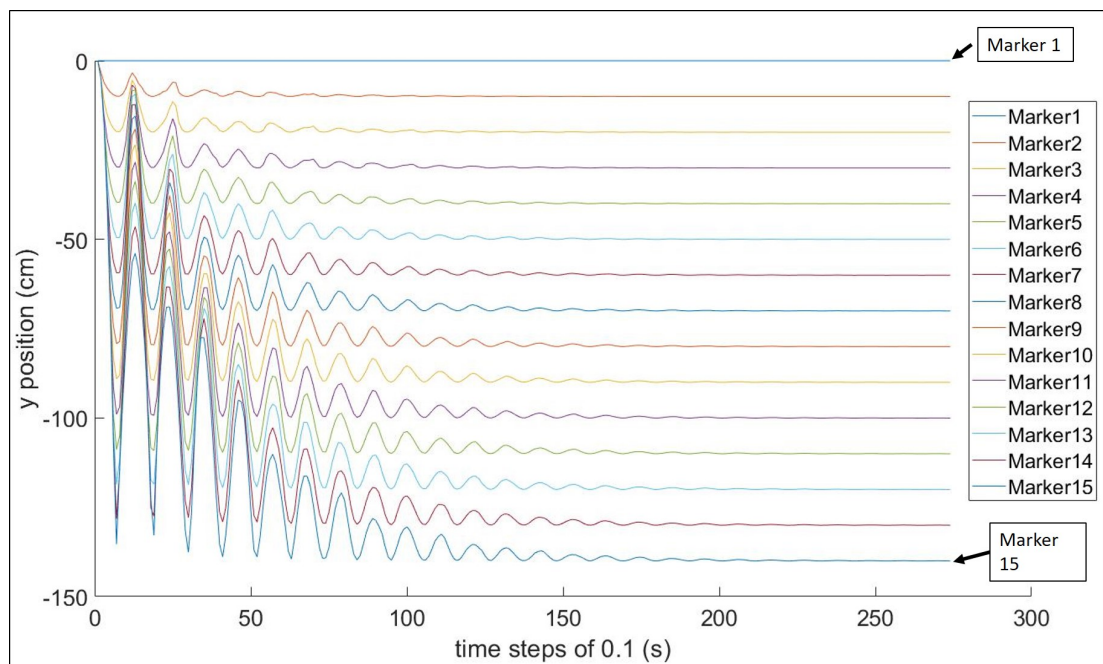


Figure 3.6: Simulated y position of each link at the defined time-steps.

Even though the values between the model and the estimation are different, it can be assumed that the tether model provides relatively accurate results because the simulation simulates the tether in a 2D plane whereas the tether in the experiment is moving in 3D. The oscillations which are visible at the later stages of both the x and y the experiment results are actually the tether moving in a circle around the z-axis.

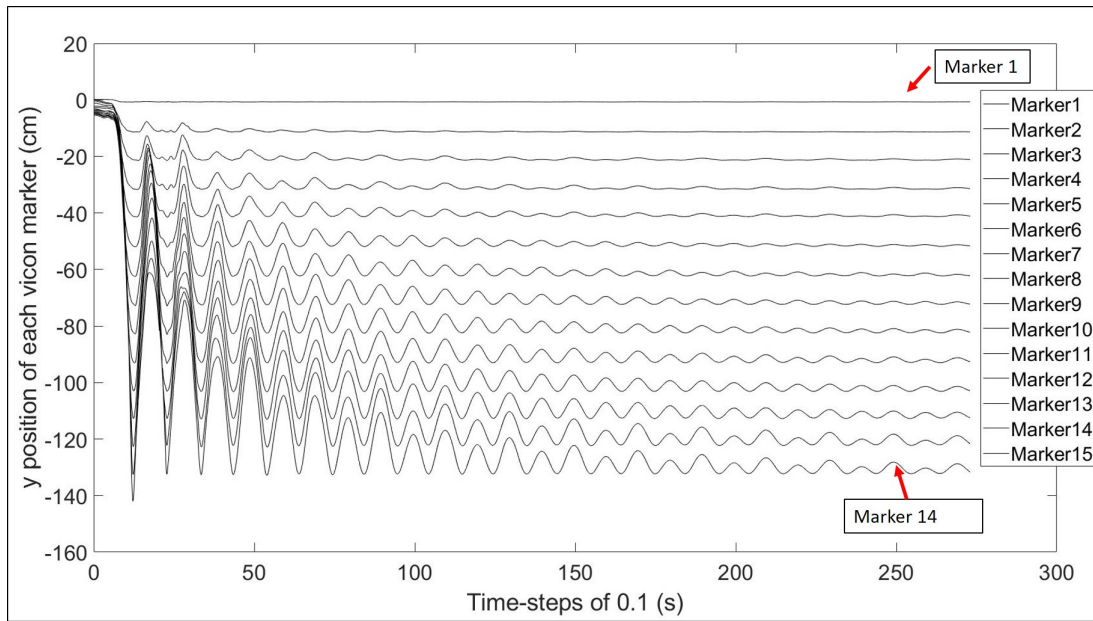


Figure 3.7: y position retrieved from the Vicon system for each marker at certain time-steps.

3.2.2 Tether Manoeuvred by Robot

After comparing the results of the tether falling due to gravity, the model was then modified in order to estimate the movements of the tether when a robot is moving along the ground in a certain direction. The viscous damping coefficient should have less effect on this model as there exists no sudden large changes in the position of the tether links as they are connected to a moving robot. In the simulation, the end point of a 1.45 m tether is given a constant force in the south-west direction. This force should pull the tether from its initial position until the tether is about to be stretched, at this point the tether should move in an approximate circular motion until it is straight in the in the south-west direction. As the robot cannot stretch the tether it would be in equilibrium in the south-west direction.

Figure 3.8 shows a snapshot of the simulation and a link to the video of the simulation running. Figure 3.9 and 3.10 show the simulated x and y positions at different time steps.

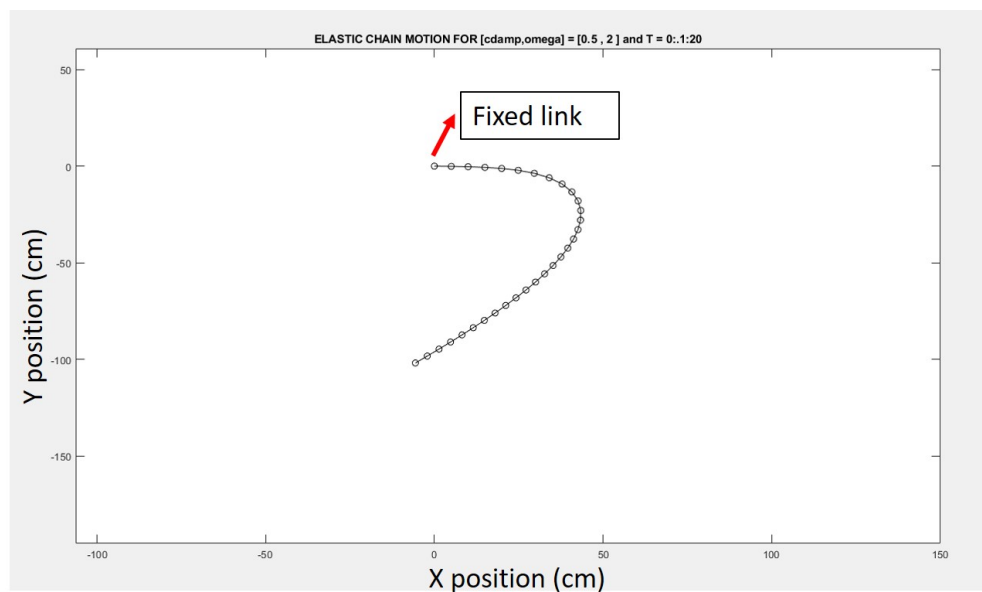


Figure 3.8: Snapshot of the simulation running as if the robot is moving the end point of the tether. Video can be viewed at: www.youtube.com/watch?v=C6cPtRLCpMo

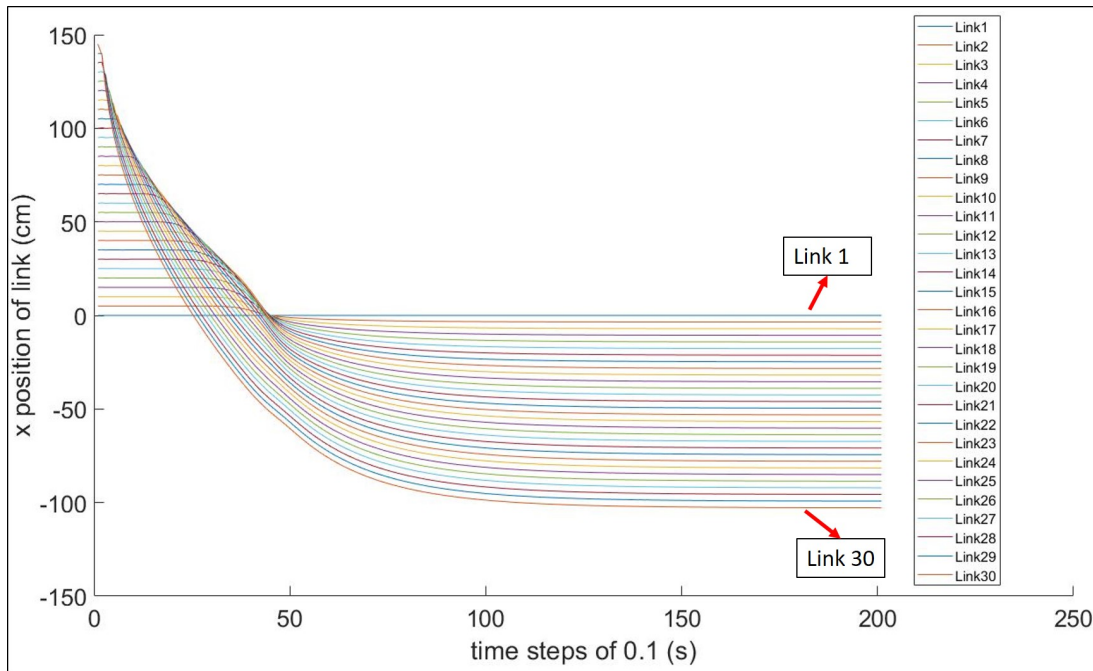


Figure 3.9: Simulated x position of each link at the defined time-steps.

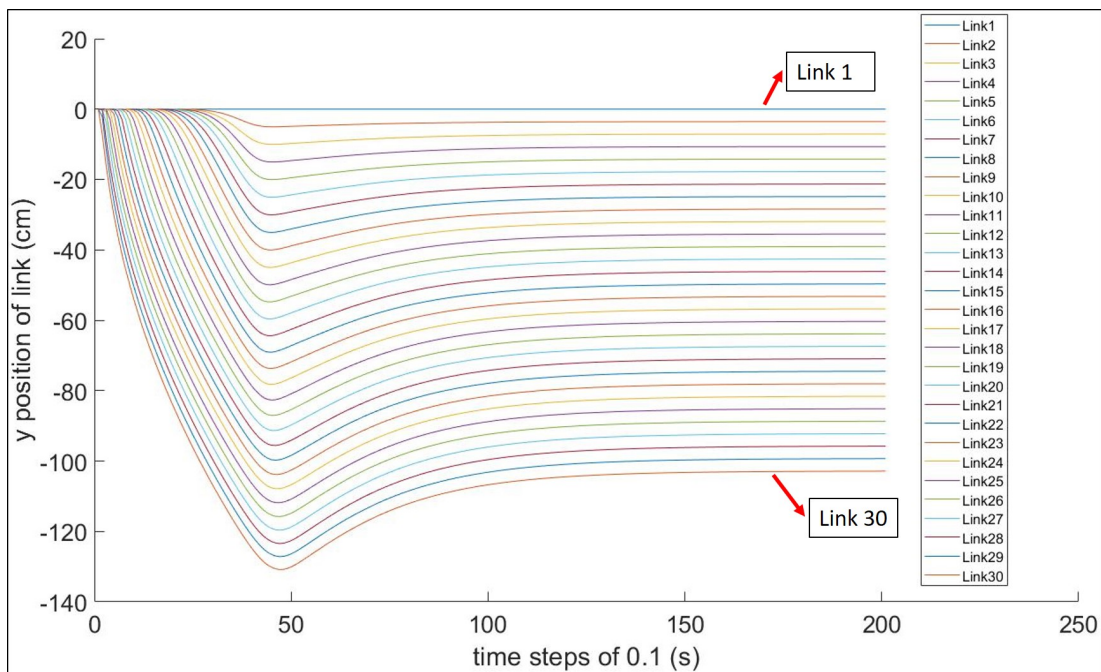


Figure 3.10: Simulated y position of each link at the defined time-steps.

From these results it can be seen that the model provides movements which correspond to the predicted movements, however its accuracy cannot be guaranteed as it has not been validated. The final position of the end point of the tether is (-102.7,-102.7) cm which corresponds to the prediction that the tether will be in equilibrium in the south-west direction. Additionally, the final position of the tether implies that its length is 145.3 cm when it is supposed to be 145 cm meaning that the tether has been stretched slightly. The confidence in this model is higher than the one for the falling tether because the movements of the end point are more stable. Additionally, the velocity of the particles is lower than the falling tether system, which implies that the effects of the damping coefficient are much lower.

3.3 Future Work

One of the physical parameters that were input into the system was the stiffness of each spring (\mathbf{K} matrix in Equation 3.1) which was estimated, however to provide more accurate data this value should be obtained. The stiffness value is very difficult to obtain for the tether because of the materials that make up the tether. A cross-section of the tether is shown in figure 3.11. The tether is made up of a composite of materials which are the tether sheath which is made of Polyurethane, the PVC wire sleeves, the twisted copper wire pairs and the empty area in the sheath. This composite of materials and the empty space in the sheathing makes estimating the stiffness of the cable difficult [87].

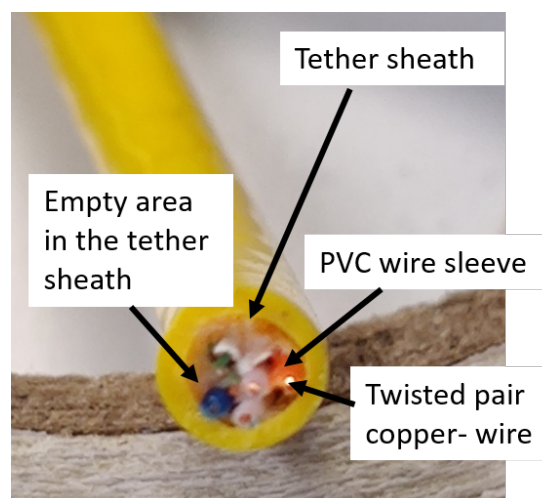


Figure 3.11: Picture of the cross-section of the tether attached to the AVEXISTM.

It is possible to experimentally obtain an estimate for the stiffness value. The stiffness (k) can be calculated using the following equation:

$$k = E \cdot \frac{A}{L} \quad (3.2)$$

Where E is the elastic modulus of the material, A is the cross-sectional area of the material and L is the length of the material. The length of the material L can be measured and the cross-sectional area A can be calculated. The elastic modulus of the material can be experimentally obtained using a tensile test experiment.

Figure 3.12 shows an illustration of how the tensile test experiment will work. A force will be applied to the tether causing it to stretch, this change in length will then be measured. The following equation can then be used to calculate the elastic modulus:

$$E = \frac{FL}{A\Delta L} \quad (3.3)$$

Where F is the force applied on the tether, L and A are the same as previously mentioned and ΔL is the change in length.

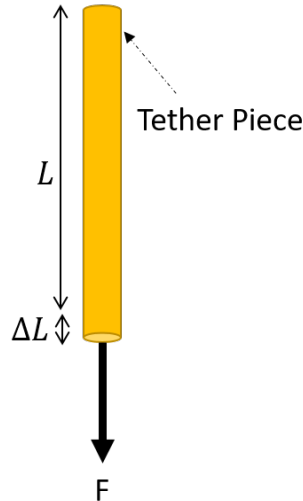


Figure 3.12: Picture illustrating the tensile test experiment.

From Equation 3.3 and the tensile test experiment it is evident that in order to obtain the elastic modulus a sufficient length of the tether is required. Therefore, the experimentally obtained estimate for the stiffness is limited to certain lengths. This implies that if the experimental value is to be used, the length of each link the simulation is limited to the length of the test specimen. This value however can only be used

as an estimate as for composite materials, as the elastic modulus alone is not sufficient to describe the stiffness [87].

The 2D dynamic model provided results that were close to how an actual tether would behave, however it did not take into account all the forces that an actual tether would experience like the tether's internal damping and restoring forces. These forces should be added to the model to provide a much more accurate tether simulation. Furthermore, this model considers the tether to be in air, therefore when an underwater tether simulation is required the other forces due to a neutrally buoyant cable need to be considered as mentioned in Section 3.1.2

Another aspect that still requires research is to obtain the effect of the tether forces on the movement of the robot. These effects will depend on the movement of the robot and whether the model is in air or underwater. The forces of the each link of the tether in the aforementioned model are calculated in order to estimate their positions however, how they effect the movements of the robot in the end is not considered.

Furthermore, the simulation was computationally demanding and required a few minutes to complete a simple simulation of a 20 cm tether for 15 seconds, hence expanding the length of the tether and the time that the simulation will run at, will drastically increase the time required for it to finish. Furthermore, expanding the system to a 3D model while also considering all the other mentioned forces, will greatly increase the computational power required.

Therefore, now that an understanding of the underlying issues with modelling a tether are known, a physics simulation package like Vortex Studio (as mentioned in Section 3.1.3) should be used to model the behaviour of the 3D model as the software should account for all the mentioned forces while also considering collisions of the tether with the environment or itself. The software capabilities could not be tested as it was too computationally powerful to run on the provided computer.

3.4 Summary

This chapter outlined and discussed the work done on the tether model and the challenges with implementing it. The three possible methods of simulating a tether were discussed.

A dynamic model of the tether was simulated and experimentally validated. The model provided data comparable to real-world experiments however some of the forces that act on the tether were not considered. Considering these forces should allow for a more accurate simulation which can then help determine the minimum number of required sampling points along the tether.

Furthermore, the model was modified to simulate the behaviour of the tether as if a robot is moving along a 2D plane. The modified model provided a simulation which visually looks correct, however it has not been validated.

Chapter 4

2D Tether Localisation System

A 3D localisation system is the requirement for the real-world underwater deployment, however to simplify the problem, the first step is to implement a 2D air localisation system, as it makes the validation and experiments viable. This can then be analysed to see the feasibility of extending the system into a 3D localisation system that can be used underwater.

This Chapter discusses and analyses a 2D plane tether localisation system.

4.1 Choosing a Sensor

In order to develop a tether localisation system that estimates the end position of the tether, sensors have to be used to measure either the end position of the tether or the physical changes along the tether. Figure 4.1 shows an illustration of how sensors along the tether can be placed to measure the bends along the tether.

By knowing the bends at different points along the tether, it is possible to estimate the end position of it, which will be discussed in more detail later on in this chapter. A 2D localisation system will only require the bend along one axis to be measured and therefore only one sensor is required at each sensing point, however, when the system is expanded to 3D, the tether can bend along all three axis and therefore it will require three sensors at each sensing point.

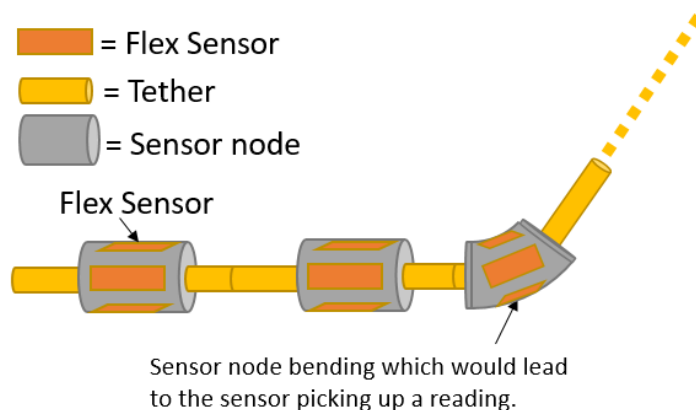


Figure 4.1: Picture showing a sketch of the sensor nodes along the tether.

4.1.1 Sensor Selection

There exists very few options for measuring the the physical changes along a tether. The choices that are currently available are:

- FBGs (as explained in Section 2.2.4), which has been excluded from the research due to its high cost and lack of published results.
- Flex sensors.
- Strain gauges.
- Image based tether localisation, which will be discussed further in Chapter 5.

Flex sensors and strain gauges work in a very similar matter. Flex sensors use flexible conductive ink printed on a flexible base, which forms a resistor. When the base bends, the conductive layer is stretched, it becomes narrower and longer. This increase in length results in an increase in the resistance, which can then be measured. Strain gauges work in exactly the same manner. Flex sensors only provide a linear relationship between the bend and resistance in one direction, therefore for a 2D localisation system two flex sensors are required to measure both directions of the bend.

Flex sensors come in two lengths; 5.537 cm and 9.525 cm, while strain gauges come in many different lengths and sizes, which make them suitable for a range of applications¹. The objective of the tether localisation system is to estimate the end point

¹<https://www.variohm.com/news-media/technical-blog-archive/what-is-a-strain-gauge->

of a 30 m tether (which is the position of the robot), this implies that there needs to be a large number of sensors on the tether to get an accurate result. Due to the added weight and difficulties in obtaining measurements from all the sensors along the tether (more details in Section 4.4), the number of sensors that can be attached to the tether is limited. Therefore, the sensors must be of adequate length to obtain measurements from the majority of the tether while also minimising the length of the tether without a sensor node. Thus, long sensors are the only viable option.

In order to calculate the number of sensors required on a tether the following equation can be used:

$$N_{o.Sensors} = \frac{L_T \Phi}{(L + s)} \quad (4.1)$$

Where $N_{o.Sensors}$ is the number of sensors, L_T is the length of the tether, L is the length of the sensor, s is the distance between sensors and Φ is the type of sensor used, which equals 1 if a strain gauge is the type of the sensor that will be used or 2 if a flex sensor is the type of sensor that will be used.

Long strain gauges are very expensive as their prices vary from £70 to £700+ [88, 89] depending on the length. Assuming a 30 m tether is used and the tether is sampled at every 20 cm (i.e. $L + s = 20$ cm), 150 strain gauges or 300 flex sensors will be required along the tether for 2D localisation. This implies that if strain gauges are to be used, the sensors of the system alone would cost approximately £10500. Furthermore, long strain gauges generally have low resistances (maximum of 350 Ω) and their behaviour for large deflections is unknown. Flex sensors on the other hand, are less accurate, but they are much cheaper at around £8.51 per sensor [90]. Therefore, the sensors for the system would cost approximately £2553. Additionally, they are designed to detect large bends and have much higher resistance (20k Ω to 125k Ω). Therefore, flex sensors were chosen for the prototyping stage of the localisation system.

4.1.2 Flex Sensor

The flex sensor shown in Figure 4.2, works in one direction (same as Figure 4.2B) and has an active length of 5.537 cm [3].

The sensor has a linear relationship between the resistance and the bend angle.

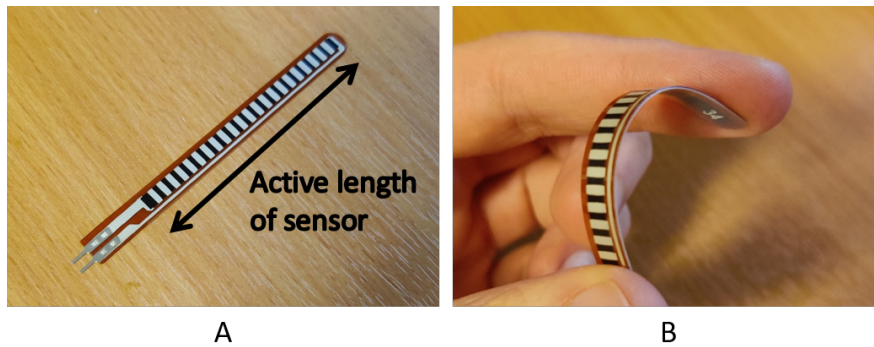


Figure 4.2: Picture of the flex sensor.

Therefore, a voltage divider circuit can be used to read the resistance using a micro-controller. The sensor can be calibrated by measuring the voltage when the sensor is straight (i.e. 0° bend), then measuring the voltage at a 90° bend (shown in Figure 4.3) and using these values to estimate the other bend angles. The angle that the sensor will read is the angle made by the the active length of the sensor, which can be looked at as an arc of a circle. This allows for geometry to be used to estimate the end position of each sensor.

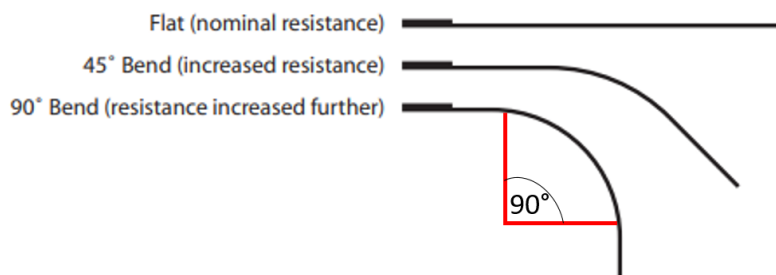


Figure 4.3: Picture illustrating how the flex sensor works [3].

Characterising the Flex Sensor

Since the flex sensor has been chosen to see if it can be used to design a low-cost 2D tether localisation system, the sensor must be characterised in order to see how it behaves. At first the sensor was calibrated as mentioned above.

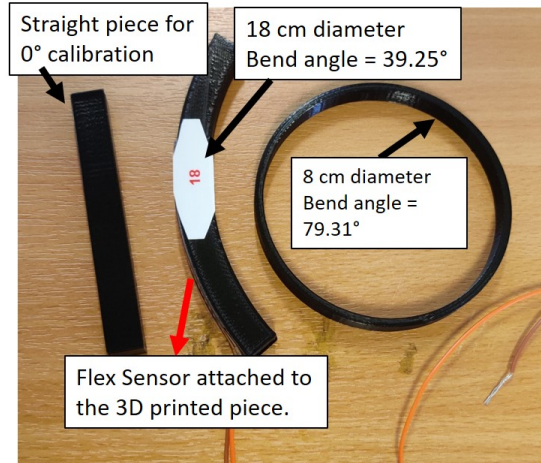


Figure 4.4: Picture of the 3D printed test pieces.

Then 3D printed circles and arcs of different diameters (shown in Figure 4.4) were used to test if the sensor provides the correct readings. The bend angle from these pieces can be calculated using the following equation:

$$D = \frac{360L}{2\pi r} \quad (4.2)$$

Where L is the active length of the sensor (5.537 cm in this case) and r is the radius of the circle or the arc. Then to quantify the error of the sensor, measurements from the sensor were obtained when the sensor was held stationary at 35.25°.

Figure 4.5 shows the time series of the measurements obtained from the sensor when it was held at 35.25°. From the obtained measurements it is possible to calculate standard deviation of the sensor measurements, which will provide an approximate error value of the sensor readings. The standard deviation can be calculated using the following equation:

$$\sigma = \sqrt{\frac{\sum(m_i - \mu)^2}{N}} \quad (4.3)$$

where σ is the population standard deviation, m_i is the angle measured from the sensor, μ is the average of the measured angles and N is the number of measurements. Using Equation 4.3 the standard deviation of the sensor was found to be 3.10°. This value

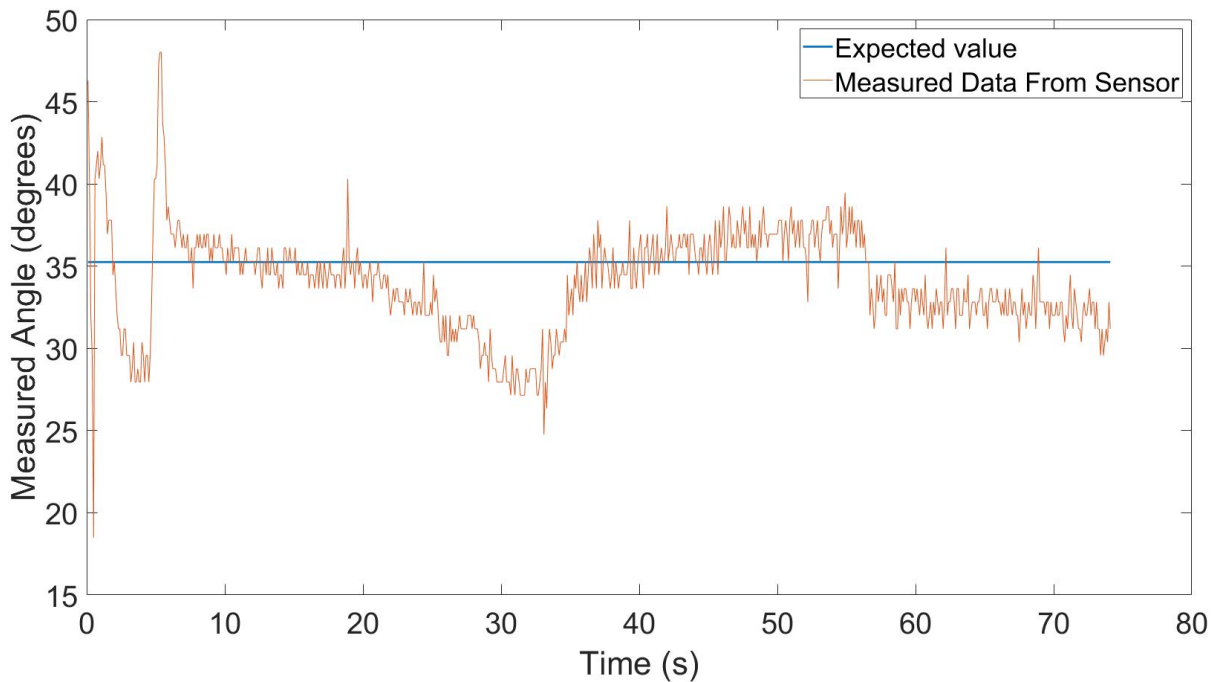


Figure 4.5: Plot of measured angles when the flex sensor is held at 35.25° .

implies that the uncertainty in the measurements of the flex sensor is 8.79%.

After calculating the standard error of the sensor, the repeatability of the measurements from the flex sensor should be tested. This is to see if the sensor will provide the same measurements for the same angle when it has been moved. To test the repeatability the sensor was moved from 0° to an angle of 79.3° and then held stationary for 75 seconds repeatedly.

Figure 4.6 shows the plot of the flex sensor measurements for each run. It is evident that the sensor measurement fluctuate significantly when the sensor is held stationary. The difference between each run is significant implying that the sensor measurements are not repeatable, this could be due to multiple factors such as that the sensor has been fatigued and that the sensor might require recalibration after each run (making it unusable in an actual tether localisation system).

Furthermore, the measured angle by the sensor assumes that the sensor measures the angle around it's middle point, whereas the sensor would provide a reading even if only the tip is bent, however to avoid damaging the sensors, this effect was not considered. In conclusion the flex sensor does not provide accurate or repeatable results,

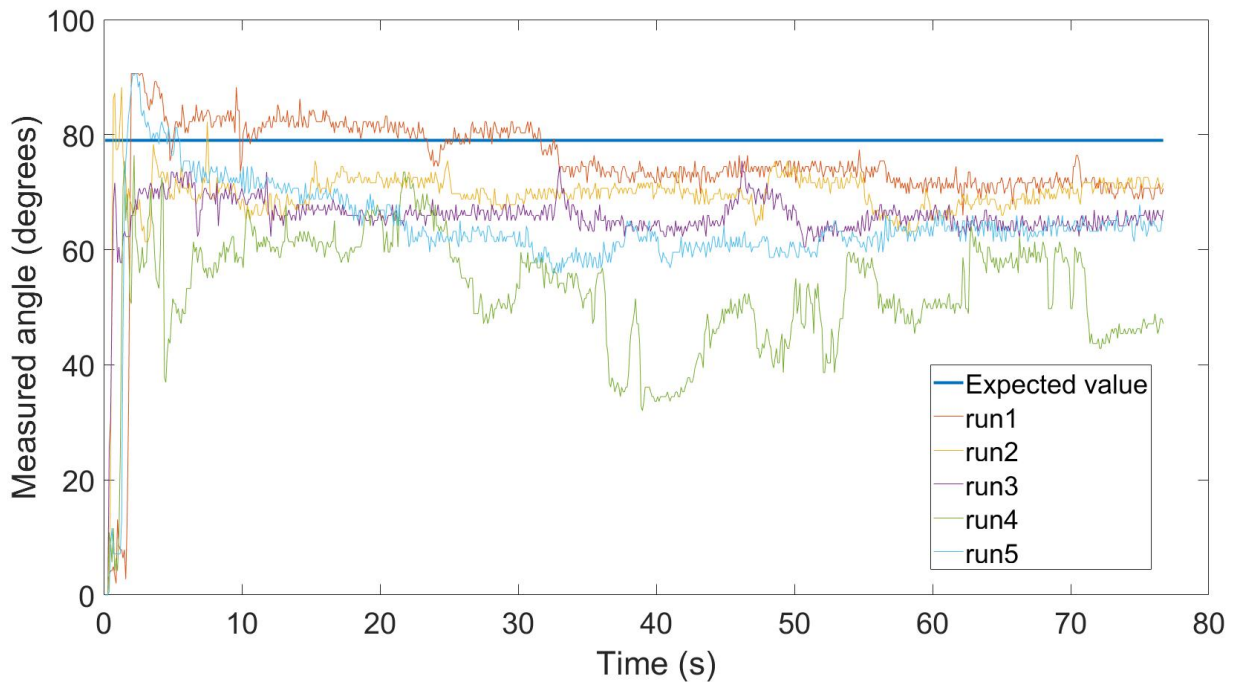


Figure 4.6: Plot of measured angles from flex sensors when moved from a straight position to an angle of 79.3° .

however it can be used to proof the concept. In the future, a better sensor might be developed which provides both accurate and precise measurements of the bends.

4.2 Theory for the Tether Localisation System

The angle that is read by the sensor is the central angle of the arc. The only known parameter is the active length of the sensor (i.e the arc length L).

Figure 4.7 shows an illustration of the flex sensor (thick line) and all the corresponding parameters that are known or can be derived from known parameters such as the radius of the circle (r), the chord length (c) and the local coordinates of the end point of the sensor (x_p, y_p).

The radius of the circle can be calculated by the following equation (θ is in radians):

$$r = L/\theta \quad (4.4)$$

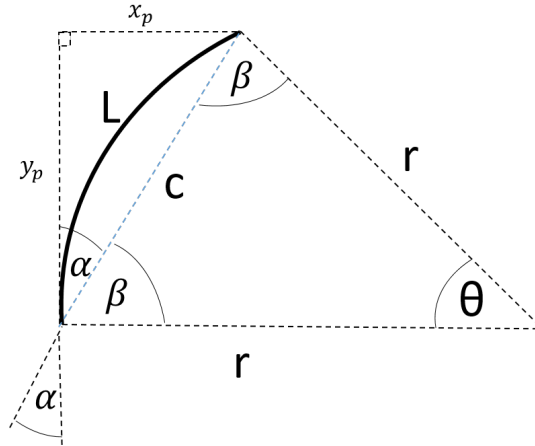


Figure 4.7: Picture illustrating the flex sensor approach.

Once the radius is known it is possible to calculate the length of the chord using the cosine rule:

$$c = \sqrt{2r^2(1 - \cos(\theta))} \quad (4.5)$$

An issue arises when the angle measured by the sensor is 0° , this means that r is undefined. Therefore, an exception was given when $\theta = 0^\circ$, the radius value is not calculated and the chord of the circle is the active length of the sensor i.e. $c = L$.

Since the chord of the circle creates an isosceles triangle, the angle that the chord (c) makes with respect to the y -axis in the local frame can be calculated using:

$$\alpha = \theta/2 \quad (4.6a)$$

Since:

$$\beta + \alpha = \pi/2 \quad \text{and} \quad \theta + 2\beta = \pi \quad (4.6b)$$

That then allows for the x and y position of the end point of the sensor to be calculated using trigonometry:

$$x_p = c \sin(\alpha) \quad (4.7)$$

$$y_p = c \cos(\alpha) \quad (4.8)$$

The previous steps mention how to get the position of the end point of the sensor in the local frame, however since the aim of this approach is to localise the end point of the entire tether and not just one sensor, they must be daisy chained together. Figure 4.8 shows an illustration of the approach of having multiple sensors one after another, where r_n is the radius of the n^{th} sensor and (x_{pn}, y_{pn}) are the positions of the end point

of the n^{th} sensor. The shape of the tether between sensors 0 and 1 shown in Figure 4.8 is unlikely to happen in reality, however it was drawn like this to illustrate the parameters clearly.

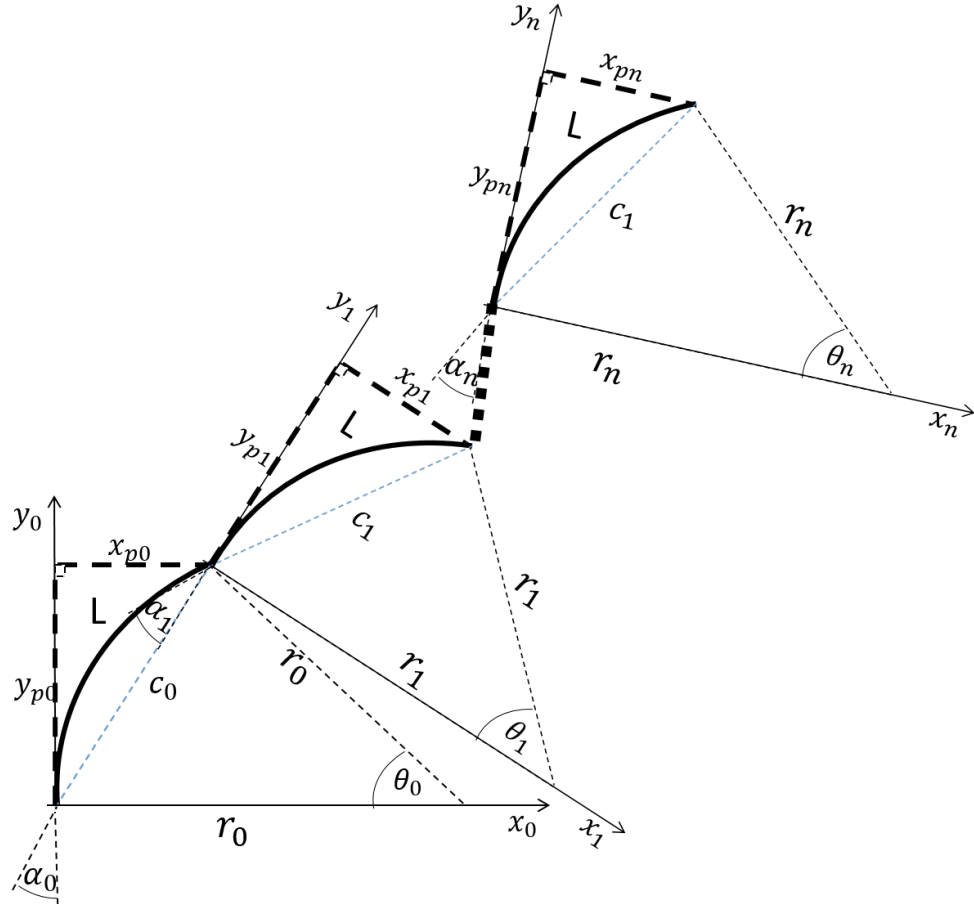


Figure 4.8: Picture illustrating multiple flex sensor approach.

However, these are the positions of the end point in the local frame and must be converted in respect to the original frame. To simplify the problem the y -axis of the local frame is assumed to always be a tangent to the segment of the circle that is created by the flex sensor. Additionally, the y -axis of the sensor is assumed to be at the same angle as the chord of the previous sensor. These assumptions allow for the homogeneous transformation matrices (shown in Equation 4.9) to be used to transform the local-frame coordinates relative to the starting frame.

$$H_n = \begin{bmatrix} \cos(-\alpha_n) & -\sin(-\alpha_n) & x_{pn} \\ \sin(-\alpha_n) & \cos(-\alpha_n) & y_{pn} \\ 0 & 0 & 1 \end{bmatrix} \quad (4.9)$$

Where α_n is the clockwise rotation of the axis, given by equation 4.6a (it is negative as it is a clockwise rotation), and x_{pn} and y_{pn} are the x and y position of the origin of the next local frame.

To get the position of the end point the Homogeneous transformation matrix must be multiplied in the correct order as follows:

$$G = H_0 \cdot H_1 \cdot \dots \cdot H_{n-1} \cdot P_n \quad (4.10)$$

Where G is the position of the end point in the starting frame, H_n is the respective Homogeneous transformation matrix and P_n is the position of the end point in the final frame, i.e:

$$P_n = \begin{bmatrix} x_{pn} \\ y_{pn} \\ 1 \end{bmatrix} \quad (4.11)$$

4.3 Simulation and Experimental Results

In order to test the model, four points were plotted on a grid and the corresponding angles were calculated and then put into the model. The length of the sensor was set to 2π (where the actual sensor is 5.537 cm) to allow for simpler calculations. The angles that were input were 0 rad, $\pi/2$ rad, $\pi/2$ rad and $-\pi$ rad, meaning that there is no rotation at the first sensor (i.e. it is along the y -axis), then a clockwise 45° rotation and then another clockwise 45° rotation and finally a counter-clockwise 90° rotation.

Additionally, it is assumed that the end of one sensor is the beginning of the next one to allow for simpler hand calculations, this is to check that the answer given by the model is the same as the expected value. Figure 4.9 shows the calculated end position points with the above mentioned parameters.

The model then calculates the end position relative to the starting frame to be:

$$P = \begin{bmatrix} 9.657 \\ 14.283 \end{bmatrix}$$

This value is the same as the calculated one hence the model provides the expected result. However, in reality it is not possible to have a large number of sensors along the tether. For a 30 m tether and an active length of 5.357 cm for each sensor there would be approximately 541 sensors placed along the tether. This will be really difficult to maintain (more detail in Section 4.4) and therefore the sensors must have a separation

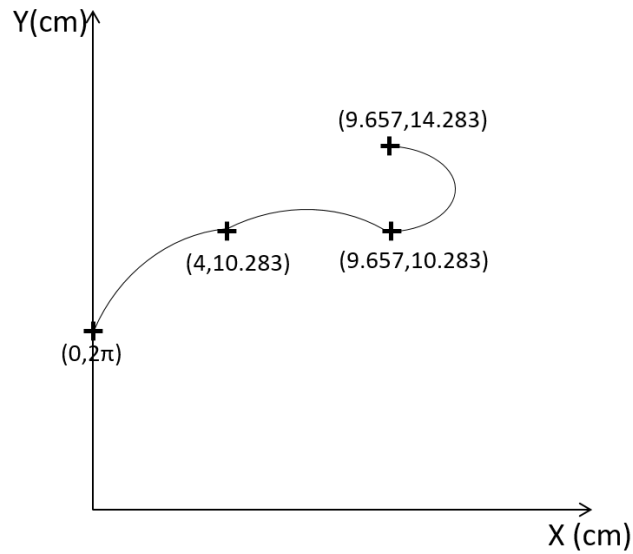


Figure 4.9: Points on grid to see if the model predicts the end point correctly.

distance between them. This separation will lead to an error in the final estimated position, as their position will have to be approximated.

To validate the proposed method a small test rig was built. Three flex sensors were placed on a 30 cm tether to provide the bend angles at different points. Figure 4.10 shows the rig, where the start and end points are pinned on to a cm grid.

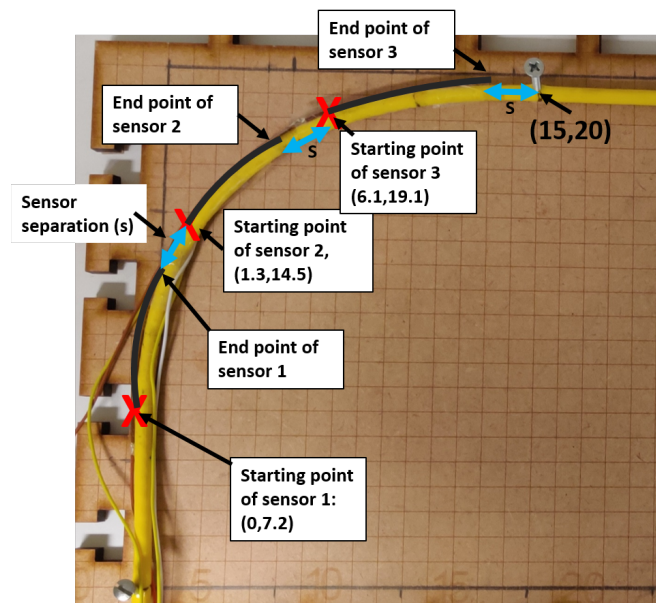


Figure 4.10: Experiment rig with three flex sensors placed along the tether.

The separation between the sensors will cause an error in the estimated position of the end point of the tether. There are four methods to deal with the separation.

One method is to assume that the separation following each sensor is a continuation of the arc of the circle at the corresponding sensor. The chord of the circle is from the beginning of the sensor to the beginning point of the following sensor, as seen in Figure 4.11.

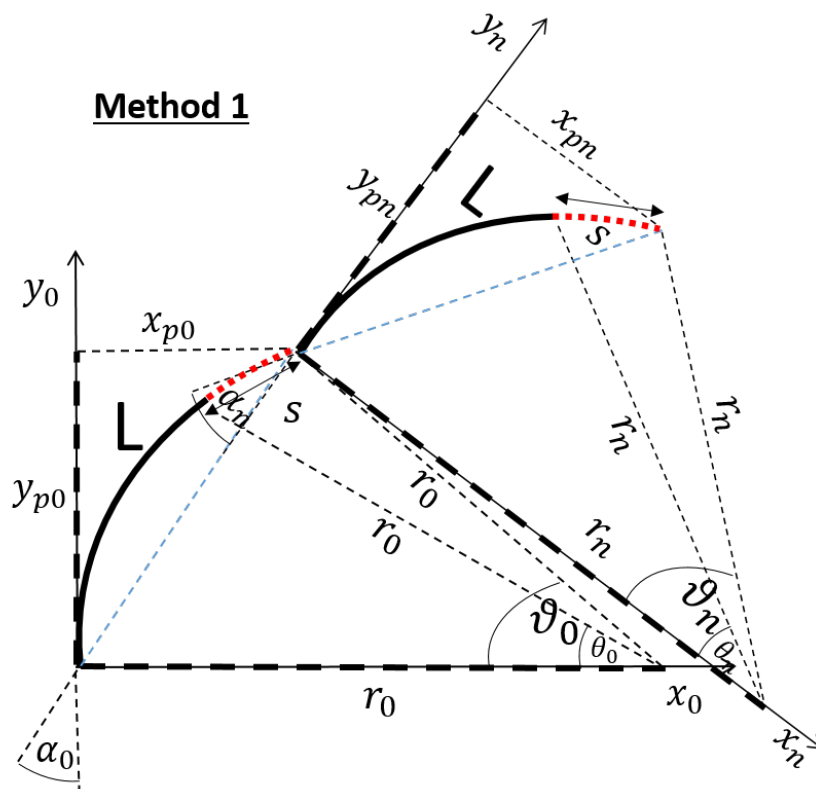


Figure 4.11: Picture illustrating multiple flex sensor approach with the sensor separation assumed to be a continuation of the arc of the circle.

The second method is to assume that the separation (s) between sensors is straight and as an extension of the chord, as seen in Figure 4.12. The assumption that the sensor separation is straight will only work for short lengths of the sensor separation s , since a longer separation will most likely be curved. A way to avoid this is to sheath the sensor separation with a stiffer material to ensure that it is kept straight.

The third method is to assume that the sensor separation is straight and a continuation of the trajectory of the tip of the sensor (not the arc of the circle). Figure 4.13 shows an illustration of the assumption.

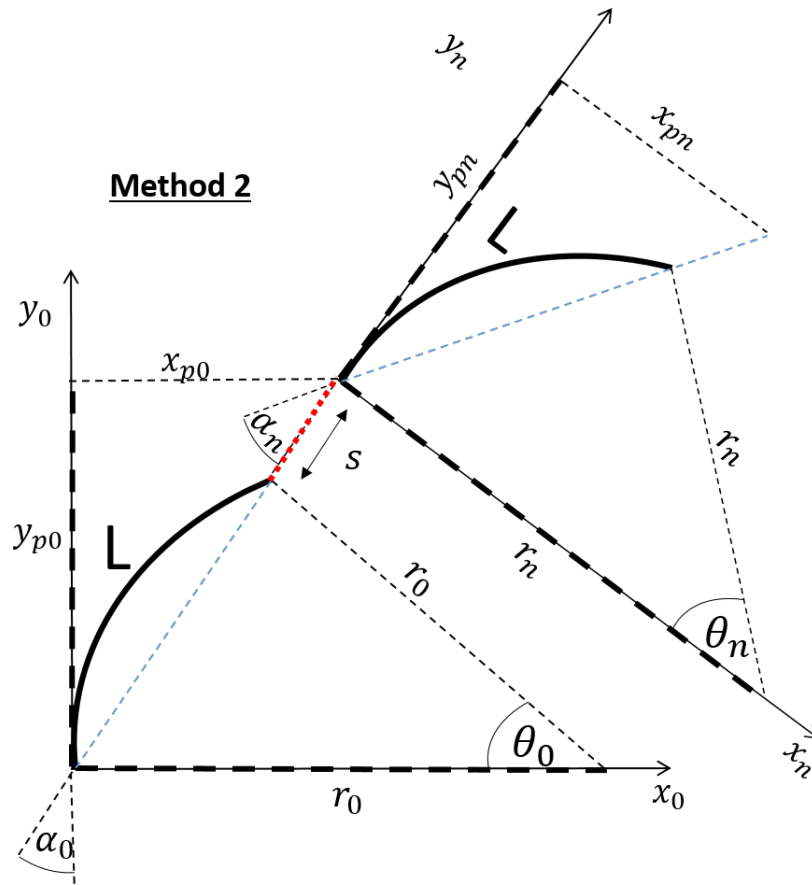


Figure 4.12: Picture illustrating multiple flex sensor approach with the sensor separation assumed to be a continuation of the chord of the circle.

To simplify the calculations, the sensor separation will be considered to be a new frame. This frame will be rotated at an angle of ϕ . Additionally, the next sensor's frame can no longer be considered at the same angle as chord of the previous sensor as the new rotation due to the sensor separation needs to be considered. The y-axis of the following sensor's frame, will have the same angle as the sensor separation as illustrated in Figure 4.14.

The final method is to assume that the sensor separation is straight and at an angle that is an average between the previous and the following sensors readings. Figure 4.14 can also be used to show the illustration of the assumption where in this case $\phi_1 = \frac{\alpha_0 + \alpha_2}{2}$. Moreover, similarly to the above assumption, the frame of the following sensor will be at the same angle as the sensor separation.

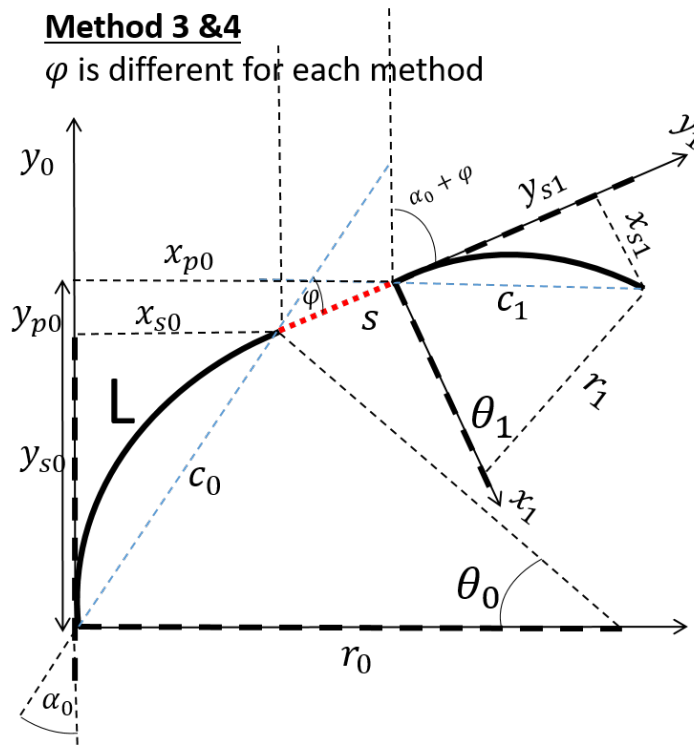


Figure 4.13: Picture illustrating the sensor separation as a continuation of the trajectory of the tip of the sensor.

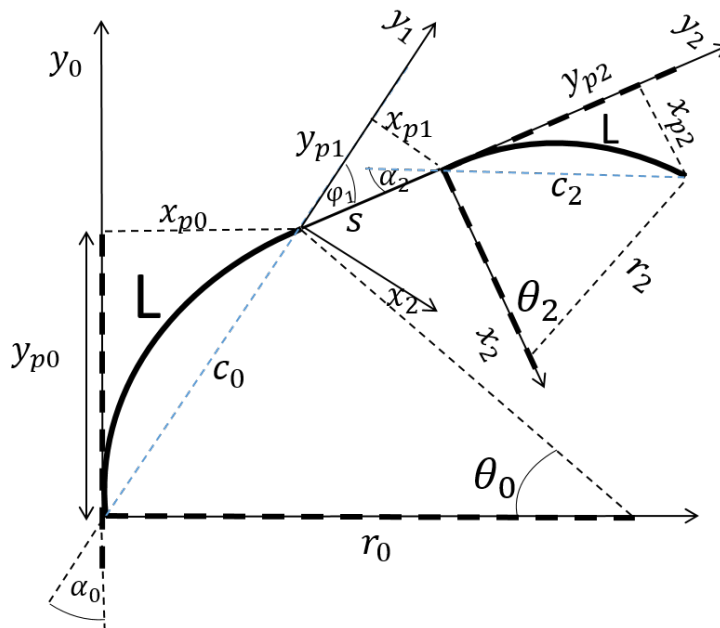


Figure 4.14: Picture illustrating the sensor separation as an additional frame.

Furthermore, the angle of the deployment for the tether must be known so that a rotation matrix can be used to give the position of the end point of the first sensor relative to a pre-set frame. Therefore, for the test rig, the first sensor was fixed approximately straight to avoid any issues measuring the deployment angle and then converting that to the pre-set frame. Additionally, the first section of the tether from (0,0) to the beginning of the first sensor, is a 7.2 cm straight piece which is added into the model as a homogeneous transformation with a rotation of 0° and a transformation of (0,7.2) cm. The location of the next sections of the tether will be done by one of the above mentioned methods.

4.3.1 Analysis of the Results From Each Method

Each method mentioned in the previous section will provide different results. To see how they differ, the tether was moved between two known end points ((15,20) cm and (15,17) cm) repeatedly and the sensor measurements were logged. Figures 4.15 and 4.16 show the results from the experiments for the position estimation of (15,20) cm and (15,17) cm respectively. The error bars are the standard deviations of the estimated x (horizontal error bar) and y (vertical error bar) positions.

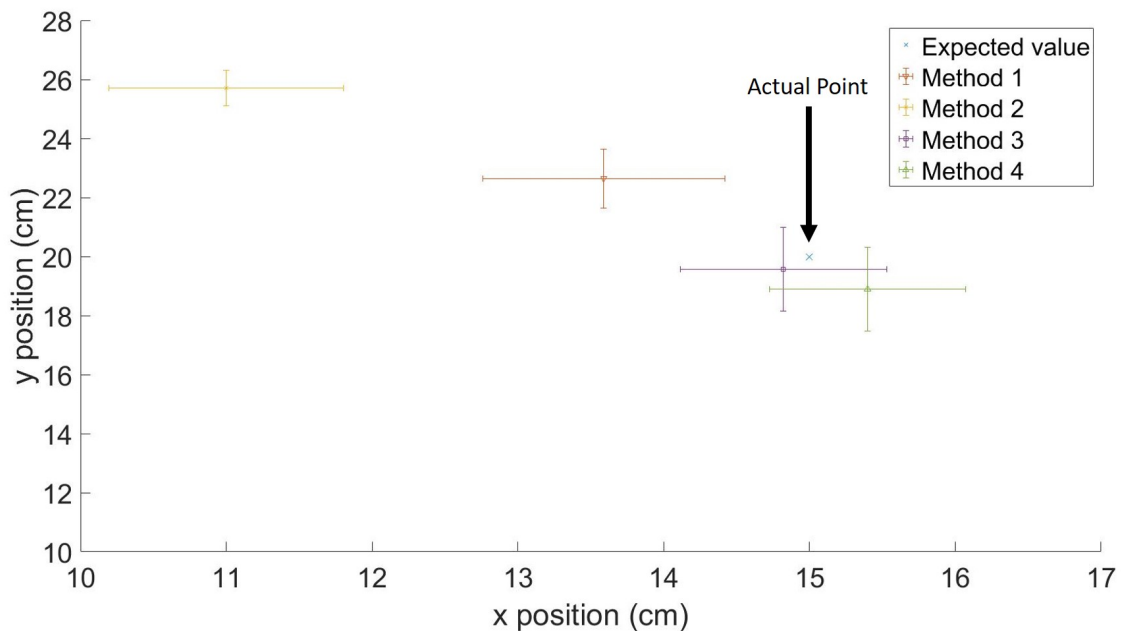


Figure 4.15: Estimated end position for each method when the end point is (15,20) cm.

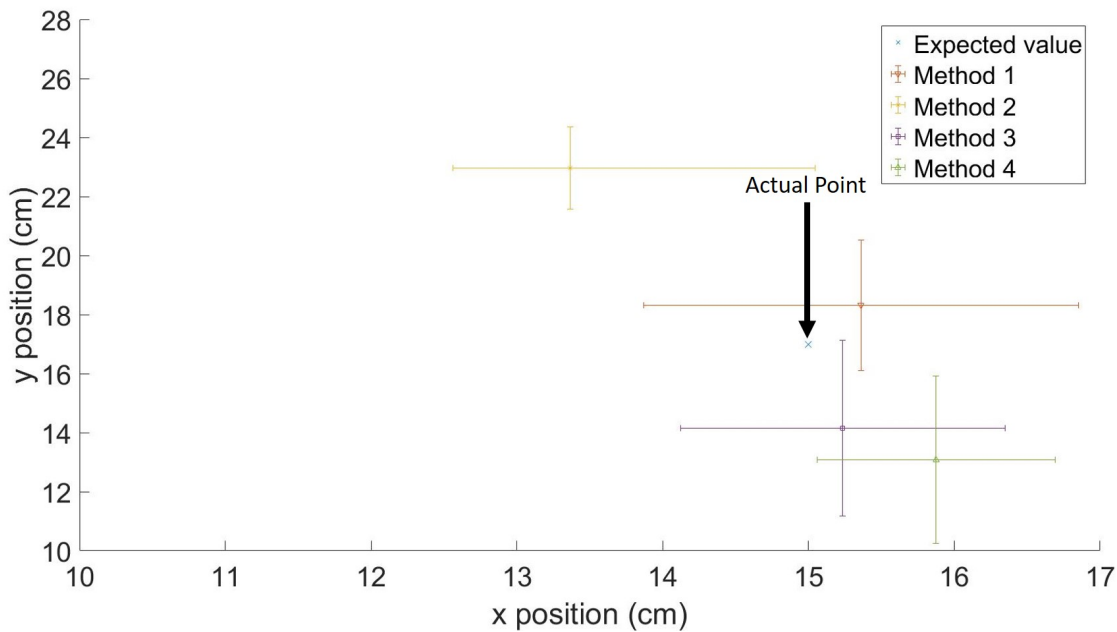


Figure 4.16: Estimated end position for each method when the end point is (15,17) cm.

For the position (15,20) cm method 3 provided the most accurate position estimation of the tether at an average of (14.82,19.57) cm which gives an absolute error of (0.18,0.43) cm. Whereas for position (15,17) cm method 1 provided the most accurate position estimation of the tether at an average of (15.36,18.32) cm which gives an absolute error of (0.36,1.32) cm. The average angles measured for position (15,20) cm were (21.8°,46.5°,24.3°) and for position (15,17) cm were (26.4°,64.4°,30.8°) which implies that when the angles are small, method 3 provides the best solution compared to when the angles are large where method 1 provides the best solution. In practice, both methods can be combined where the estimator can process small angles using method 3 and large angles using method 4.

Method 4 compared to method 3 was more precise, however it was inaccurate in comparison. Additionally, overall method 2 provided the most precise estimations however, it was the least accurate. The results shown in this section are for a 30 cm tether piece, if the system is expanded to any tether of a longer length, the estimations are expected to be less accurate and precise.

Furthermore, the assumption that the sensor separation is straight in methods 2,3 and 4 provides another source of error for the model. A possibility to increase the

accuracy and confidence in the result is to ensure that the separations are forced to remain straight by adding sheathing around them. This however, will affect the manoeuvrability of the robot but it might provide more accurate results as it will limit the sections between sensors from bending. Additionally, in the model it is assumed that the sensors bend around their middle point, where in reality this bend can start at any part of the sensor.

4.3.2 Error Propagation From Sensor Measurements

The results in the previous section did not consider the uncertainty in the measurements provided by the sensors. The errors in the measurements will propagate throughout the system as an uncertainty in the end position of one sensor will lead to a bigger uncertainty in the end position of the second sensor. The error propagation can be formulated.

If R is a function of X and Y , written as $R(X,Y)$, then the uncertainty in R is obtained by the partial derivatives of R with respect to each variable multiplied by the uncertainty in that variable and these terms are added in quadrature, this can be expressed as [91]:

$$\sigma R = \sqrt{\left(\frac{\partial R}{\partial X} \cdot \sigma X\right)^2 + \left(\frac{\partial R}{\partial Y} \cdot \sigma Y\right)^2} \quad (4.12)$$

Assuming that there are no sensor separations and ignoring the errors due to the assumptions made in section 4.2, the end position of the tether can be expressed as a function of the measured angles i.e. $G = f(\alpha_0, \alpha_1, \dots, \alpha_n)$, where G is the end position and $\alpha_n = \frac{\theta_n}{2}$. This implies that the uncertainty in the end position estimation can be expressed as:

$$\sigma G = \sqrt{\sum_{i=0}^n \left(\frac{\partial f}{\partial \alpha_i} \cdot \sigma \alpha_i\right)^2} \quad (4.13)$$

Where σG is the uncertainty in the end position, $\frac{\partial f}{\partial \alpha_i}$ is the partial derivative of the end position function with respect to α_i and $\sigma \alpha_i$ is the uncertainty in the measured angle, which was found to be 3.10° for θ

From Equation 4.13 is it evident that the more sensors there are in the system, the higher the uncertainty in the estimated position. To see how this propagates due to the sensor measurements, let's assume that a tether of approximately 30 m length is

deployed along the y -axis where all the sensor provide a reading of 0° , there will be approximately 541 sensors placed along the tether without any separation. Taking the uncertainty into account, the measurements of the sensor will be given as $\theta_n \pm 3.10^\circ$. Then the model was run for 1 million iterations with the measurement of the sensor given as $\theta_n \pm rand \cdot 3.10^\circ$, where $rand$ is a random number between -1 and 1. Figures 4.17 and 4.18 show the normal distribution of the error in both the x and y estimated positions respectively, where the darkly shaded region specifies the area which 68% of the values are within (i.e. 1 standard deviation).

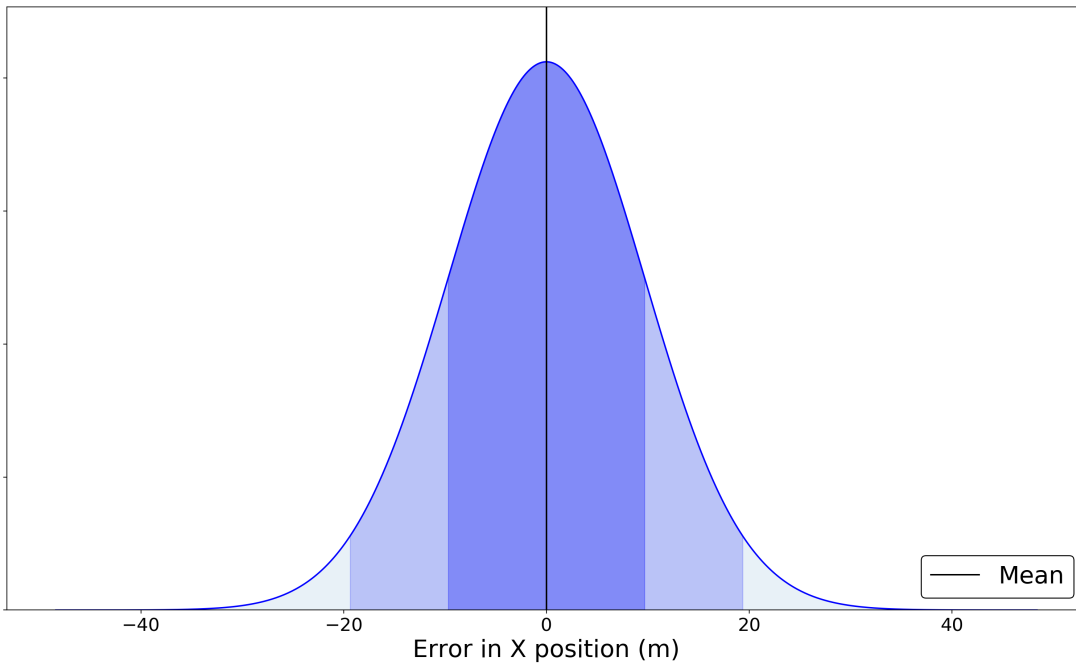


Figure 4.17: Error distribution for the x position estimations.

From the results it was found that for the y estimated-positions the absolute average error was 2.79 m and the standard deviation was 3 m, whereas for the x estimate positions the absolute average error was 0.01 m and the standard deviation was 9.68 m. It is clear that the inaccuracy of the system in the y position estimation is relatively large compared to the x position, this is due to the fact that it was assumed that the tether was deployed along the y -axis, whereas if it was along the x -axis, the opposite behaviour is expected. Additionally, the uncertainty in the y position is approximately 3 m which is 10% of the length of the tether, whereas the uncertainty in the x position is approximately 9.7 m which is 32% of the length of the tether. These values imply that the error in the system propagates largely making the system unfeasible using the current sensors.

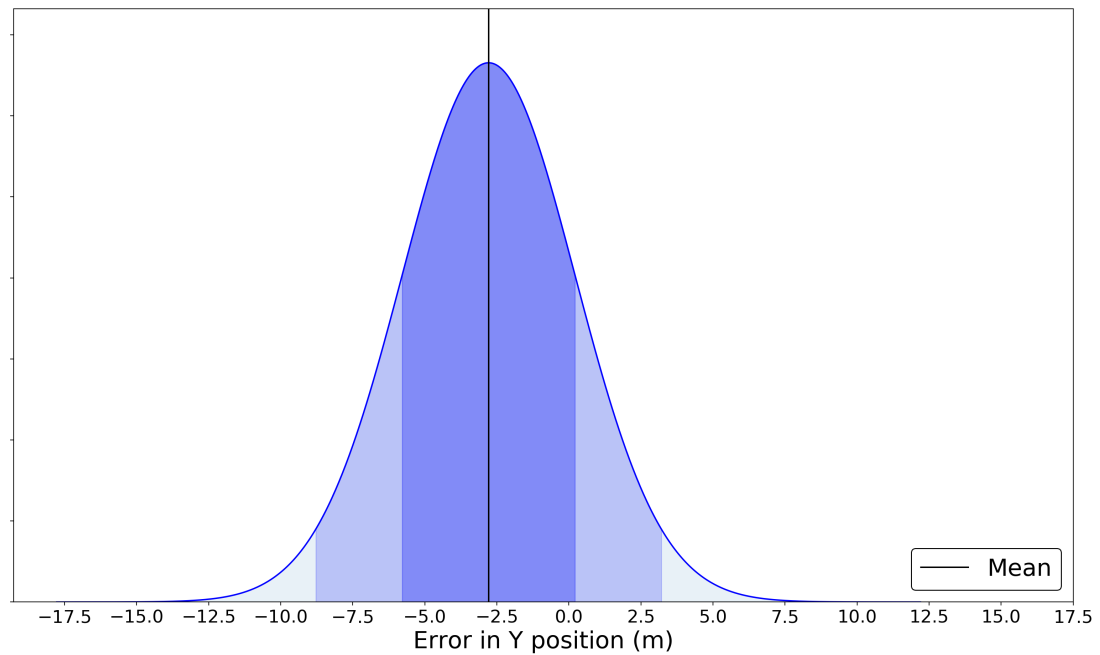


Figure 4.18: Error distribution for the y position estimations.

The error analysis above is for the flex sensors that were chosen for this proof-of-concept system. However, it is possible to estimate the required precision of a sensor that can provide the required precision mentioned in Chapter 2. The sensor separations for such an estimation cannot be ignored and therefore, the sensor separation is set to 4.463 cm, this implies that the tether gets sampled every 10 cm. Assume as above, that a tether of approximately 30 m length (meaning that there will be 300 sensors along the tether) is deployed along the y -axis where all the sensors provide a reading of 0° and the estimation for the sensor separation position uses method 3 mentioned in Section 4.3. Figure 4.19 shows the uncertainty in the x position estimation for varying uncertainty of sensor measurements. The uncertainty in the y position was not considered as due to the assumption that the tether is deployed along the y -axis it will be low, this is because the y position estimation uses cosine and since the angles are very small, the variations in the estimated y position will be small.

Since the precision required by the system is ± 0.1 m, from Figure 4.19 it is evident that the sensor must have a very low uncertainty in the estimated measured angle. It was calculated that an uncertainty of $\pm 0.02^\circ$ in the measured angle will lead to approximately an average absolute error of (0.78, 0.28) mm and an uncertainty of $\pm(0.10, 0)$ m

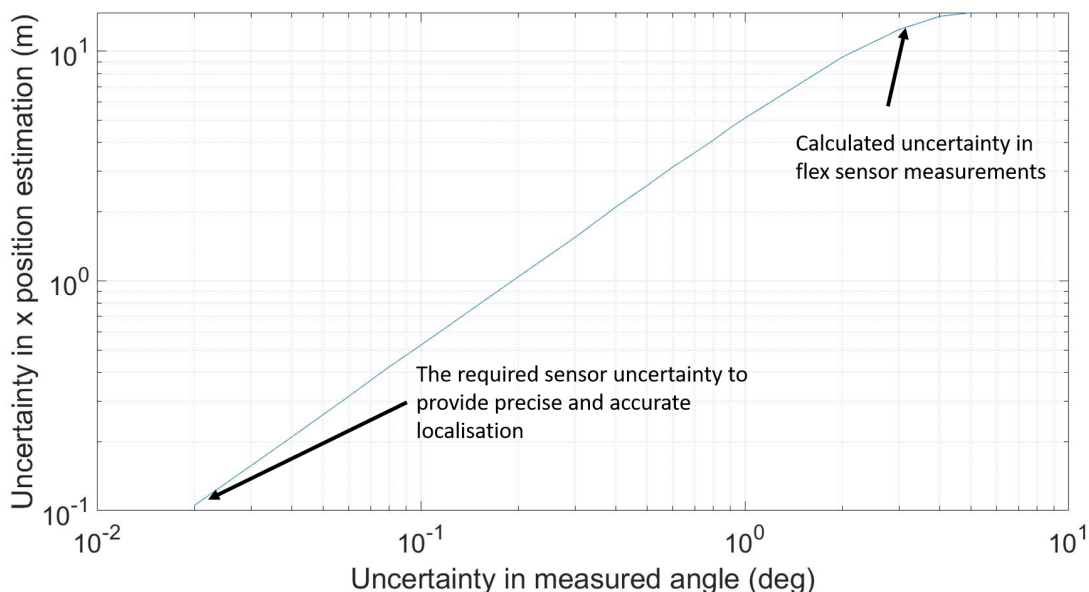


Figure 4.19: Log plot of the uncertainty in x position estimation of a 30 m Tether for varying sensor precision.

which would meet the target mentioned in Chapter 2.

4.3.3 Error Due to Sensor Separation Assumption

The previous Section explored the propagation of the error due to the measured angles.

This section will focus on the error that could arise due to any small deflections or inaccuracies in estimating the behaviour of the tether between sensors (i.e. the sensor separation sections). The sources of error for this localisation system are the values retrieved from the sensors, the measured length of sensor separations and the assumptions that were mentioned above (each method, and the y -axis of the following sensor is at the same angle as the chord of the previous sensor or the sensor separation). However, this section will only focus on the error that could be caused by the wrong assumption of the angle that the sensor separation will be at, when the sensor separation is forced to be straight at all times (by adding sheathing between sensors). Therefore, the error due to the sensor readings is ignored.

When a tether is deployed, the parts with sensors can all coincidentally read a value of 0° if they are all straight, however the sensor separation sections can vary at a very

small angle which cannot be measured by any of the sensors. This then leads to a difference between the actual end position and the estimated end position. Figure 4.20B shows an exaggerated example of this error (γ).

Assume that the tether is deployed in the plane where all the sensors provide a reading of 0° . All the methods mentioned in Section 4.3 will assume that the sensor separation is along the y -axis, meaning that the estimated end position will also be along the y -axis as seen in Figure 4.20A, where in reality it will be at a different position as seen in Figure 4.20B.

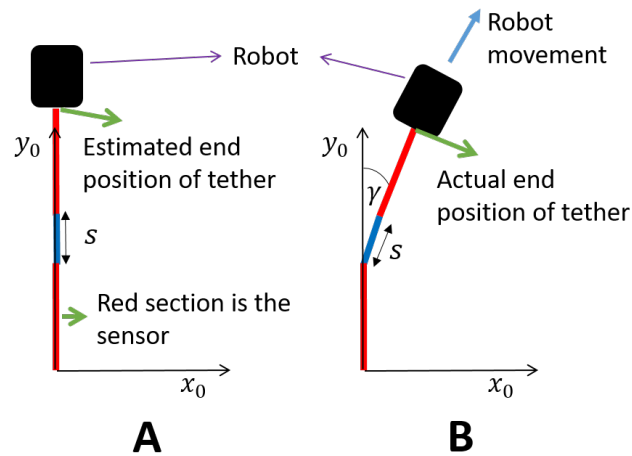


Figure 4.20: Picture illustrating the sensor separation error γ .

To see the effect of gamma on the estimated starting position of the second sensor, it is assumed that the tether is deployed along the y -axis and there is no bend in the sensor, meaning that the value of c is equal to the active length of the sensor (L), i.e. $c = L$. Additionally, the sensor separation (s) is set to 4.463 cm, which implies that the tether is sampled at every 10 cm since the active length of each sensor is 5.537 cm. This means that when γ is 0° i.e. the sensor separation is at the same angle as the sensor, the value of the end point (x_{p0}, y_{p0}) is at (0,10) cm. Figure 4.21 shows an illustration of the example.

From Figure 4.21, it is evident that if the sensor separation is in reality at an angle of γ , the actual end position of the tether section that includes the sensor and the sensor separation will be different to the one given by the model.

The gamma value will then have to be accounted for in the model mentioned in section 4.2.

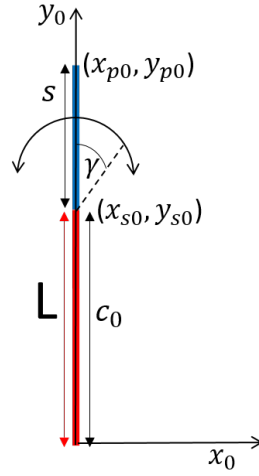


Figure 4.21: Picture illustrating how γ affects the end position of a single sensor, where (x_{s0}, y_{s0}) is the end position of the sensor and (x_{p0}, y_{p0}) is the end position of the sensor including the sensor separation.

Using equations 4.7 and 4.8, x_{p0} and y_{p0} shown in Figure 4.21 can be written as:

$$x_{p0} = c_0 \sin(\alpha_0) + s \sin(\alpha_0) = x_{s0} + s \sin(\alpha_0) \quad (4.14)$$

$$y_{p0} = c_0 \cos(\alpha_0) + s \cos(\alpha_0) = y_{s0} + s \cos(\alpha_0) \quad (4.15)$$

α_0 in this case is zero since the sensor is straight. Adding the uncertainty γ into the model gives:

$$x_{p0} = x_{s0} + s \sin(\alpha_0 + \gamma) \quad (4.16)$$

$$y_{p0} = y_{s0} + s \cos(\alpha_0 + \gamma) \quad (4.17)$$

Once the value of γ has been added to the model, it is possible to see how the value of the end position will change for varying γ values. When γ reaches 90° , the error in x and y should be the same, this error would be equal to the length of the separation distance. Figures 4.22 and 4.23 show a plot of the error in the x and y position respectively for varying values of γ . As expected, the error in the x and y position increases as γ increases. The error in the end point position when γ reaches 90° is (4.463, -4.463) cm, which is the same as the sensor separation length which is what was expected. The value of γ in practice should be very small, because any large bend in that section will most likely cause a reading to be picked up by the previous flex sensor.

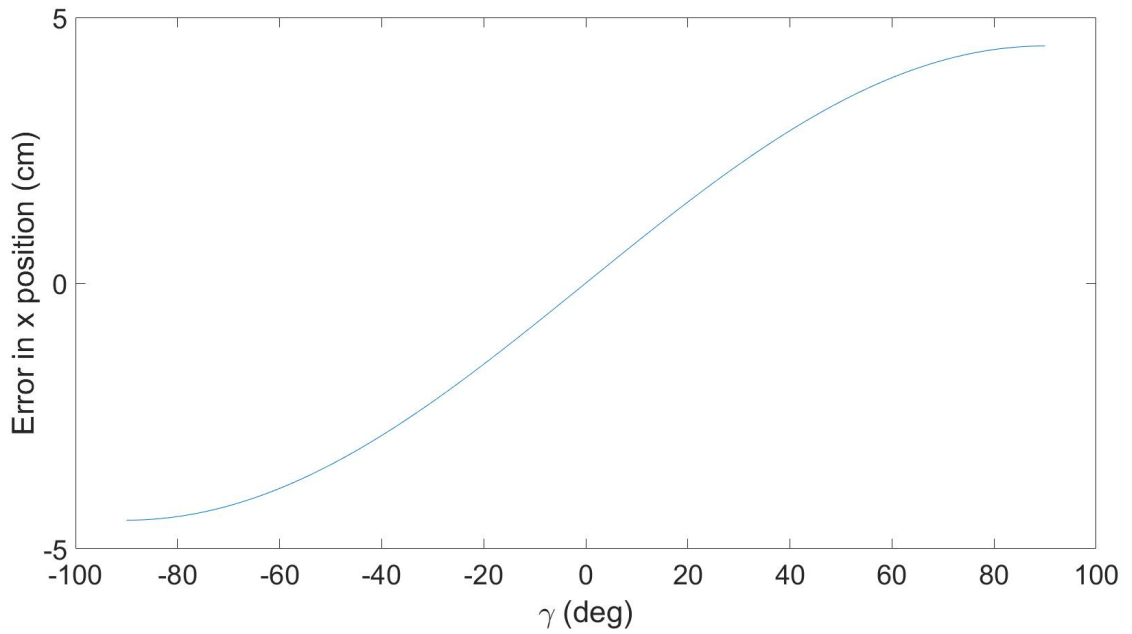


Figure 4.22: Plot of the error in the estimated x_{p0} position for varying γ values.

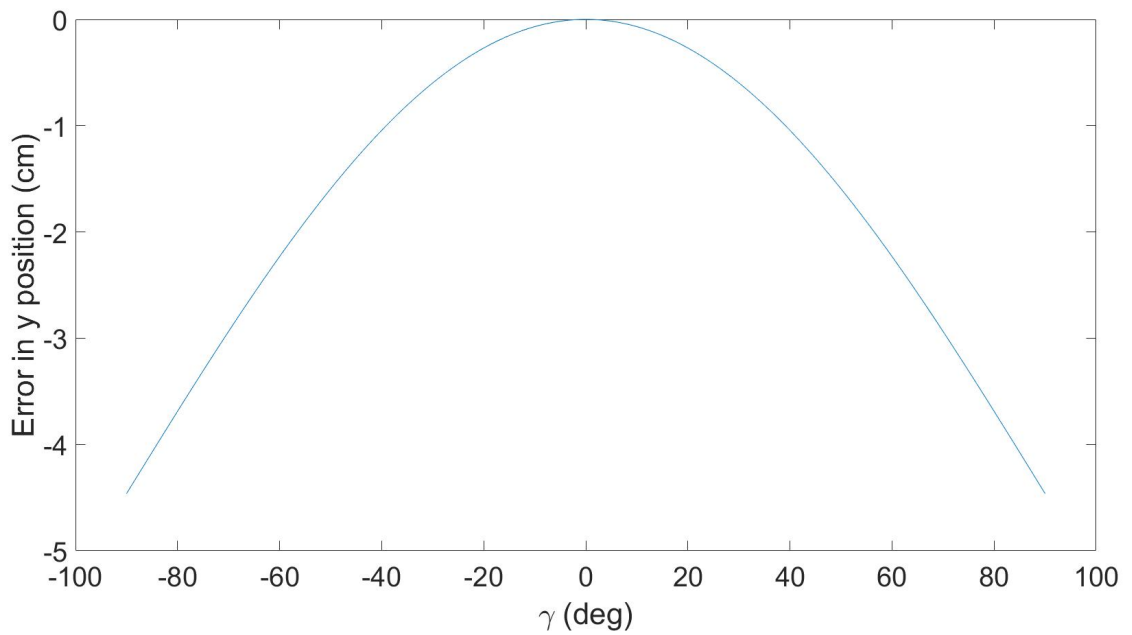


Figure 4.23: Plot of the error in the estimated y_{p0} position for varying γ values.

These error results are only for one sensor, therefore an analysis of how this error will propagate throughout the system will have to be considered. Since there is an uncertainty in the estimated position of the starting point of the second sensor, the uncertainty in the following sensors estimated position will be greater. Figure 4.24 shows a sketch explaining this point. The purple arrow approximately represents the uncertainty in the position of the end point of the sensor due to different γ values. The uncertainty in the end position of the tether will increase for each sensor.

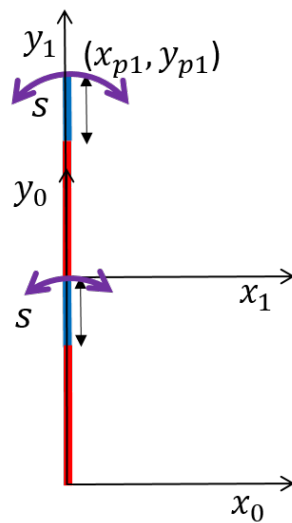


Figure 4.24: Picture illustrating the sensor separation error propagation, where the purple arrow approximately represents the uncertainty in the position of the end point of the sensor at different γ values.

To see how much this error will propagate throughout the system, a worst case scenario will be looked at, where all the sections of the tether will have the same value of γ added on to them. This implies that the tether is in reality spiralling towards its origin as illustrated in Figure 4.25.

In order to see the biggest effect of γ on the model, assume that a 30 m tether is placed in the plane spiralling inwards where the bends only occur at the sensor separation section, where each section experiences the same bend γ . Additionally, let's assume that γ varies between 0° and 1° . The sensor separation was set to 4.463 cm and the sensors read a value of 0° since no bends occur at their location. This implies that the estimated end position of the tether will be at (0,30) m. To see how the error due to γ propagates through the model, the mean squared error (MSE) along the tether can be

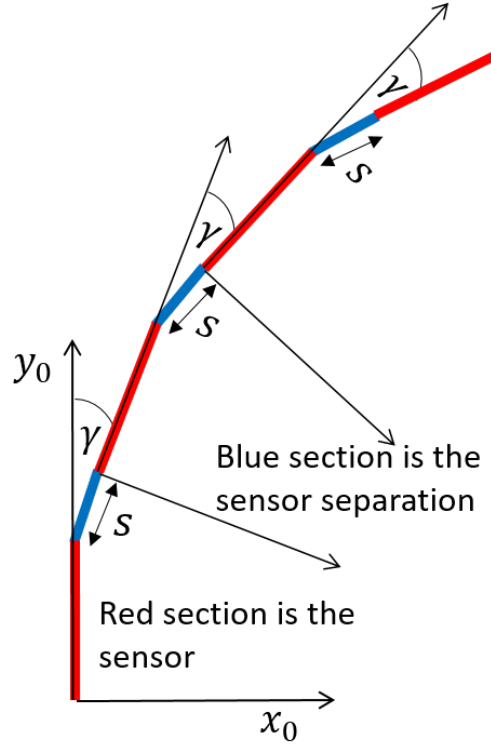


Figure 4.25: Picture illustrating the γ propagation through the entire tether, assuming that γ will be present at all points.

calculated. The MSE is a measure of the quality of the position estimation. The MSE for both the x and y positions can be calculated using the following equation:

$$MSE = \frac{1}{n} \sum_{i=1}^n (K_i - \hat{K}_i)^2 \quad (4.18)$$

Where n is the number of data points, which in this case is 600 as the sensor separation is considered as a new data point, K_i is the actual position (x or y) of the i^{th} section of the tether (spiralling inwards) and \hat{K}_i is the position (x or y respectively) that the model predicts for the i^{th} section of the tether.

Figures 4.26 and 4.27 show the mean squared error (MSE) plots in the x and y positions respectively for different values of γ .

The errors are obviously very large and that is for very small variations in the estimated sensor separation angle. This implies that the estimation of the sensor separation angles must be very precise or the confidence in the position estimation will be very low.

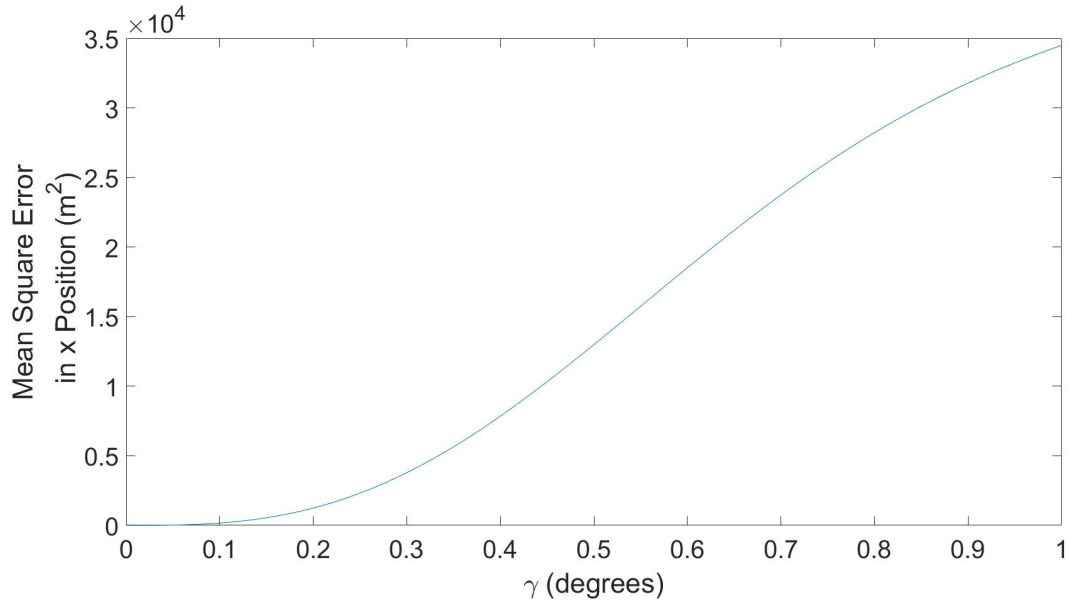


Figure 4.26: Plot of the MSE in the x values for varying γ values.

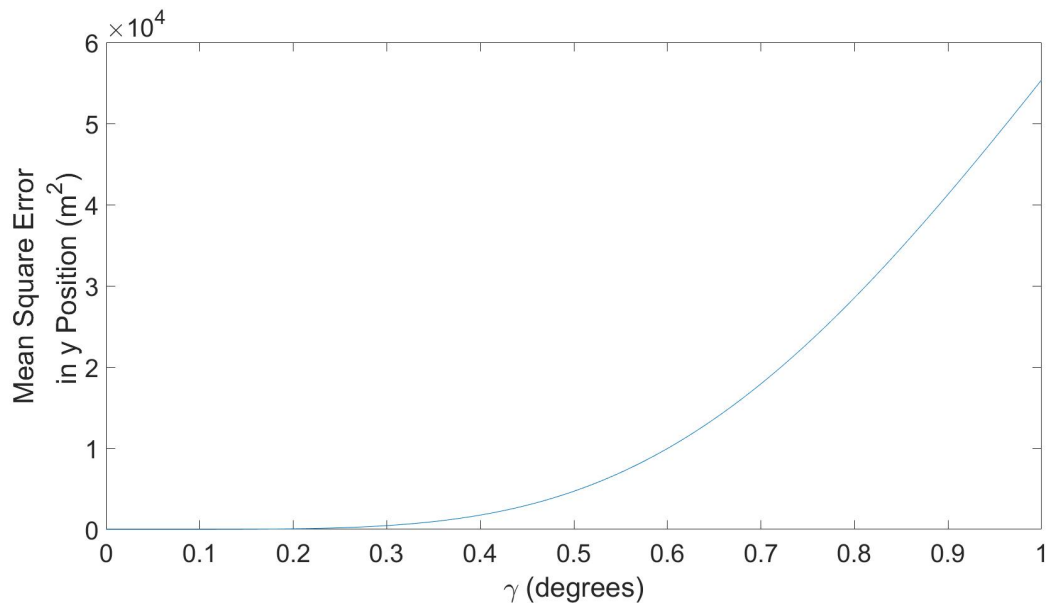


Figure 4.27: Plot of the MSE in the y values for varying γ values.

This section has looked at the effects of γ on a tether that was assumed to be straight since all the sensors provide a reading of 0° . This was to see the worst case scenario where in reality the likelihood of all the sensors reading a value of 0° when the robot is moving is low.

When the angles measured by the sensors are different to 0° , the sensor separation will be assumed to be at a certain angle (depending on the method used), this assumption will have an inherent inaccuracy dependant on the length of the sensor separation sections. This section did not have a look at these errors as it was quite evident with the first case that even a very small uncertainty in the estimated value, will cause a very large uncertainty and error in the estimated end position of the tether.

4.4 Challenges with proposed method

The researched proposed method while theoretically possible has too many downfalls, difficulties and areas of added inaccuracy to be investigated further. The idea of the 2D localisation system is to investigate whether the system would be feasible and can be expanded into a 3D localisation system. There were several challenges associated with the model and the chosen sensors. Additionally, further challenges will arise when expanding the system to a longer tether or a 3D tether. This section explains some of these issues, why they would occur and a possible way of fixing said issues.

Flex sensors are unreliable as they will not always give the same value for the same bend (as seen from the previous results) and their value fluctuates a lot even when held stationary. To help account for this issue, the average of 20 values was used to obtain the measurements used for the experiment. Additionally, they only provide a linear relationship between resistance and bend angle in one direction and hence to get accurate readings of bends in both directions, two of the sensors will need to be placed (one on each side) to get the most accurate result. Two sensors will cover the surface of the tether (as the width of each one is 0.635 cm). Therefore, if the system is to be expanded into a 3D localisation system there has to be 6 sensors (2 for each axis) placed along the surface of the tether at each sampling point. This implies that the surface of the tether needs to be expanded by a considerable amount.

Due to how these sensors operate, there exists no method of knowing the starting point of the bend. So it can start from half way through the sensor, the top or at the

beginning thus providing inaccurate results, since the model assumes that the bend is along the entire active length of the sensor. This leads to a really high inaccuracy in the results. Furthermore, another issue with these sensors is that if they experience any torsion, their resistance value could change and it will be difficult to distinguish this from its expected rotation. This can lead to further inaccuracies in the estimated final position. A possible way to avoid this issue is to house the sensors in a flexible material that would limit the effect of torsion on the sensors, since the material would twist with the tether while leaving the sensors unaffected. Figure 4.28 shows an example of how the sensor sheath will look like if implemented.

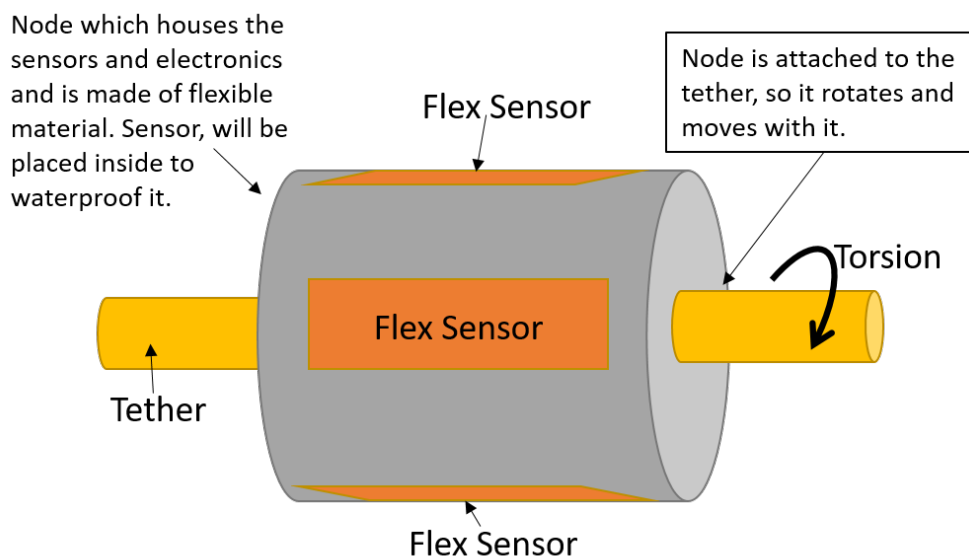


Figure 4.28: Illustration of sensor node that houses the flex sensors.

Each sensor requires calibration before being used and when more than 200 of them will be added to the system, it would require a lot of time to calibrate each sensor individually. Additionally, the sensors are very prone to damage, especially at the base of the sensors (section before the active length of the sensor begins) and when they are applied to a tether which will be reeled, they are very likely to be damaged over time and therefore stop behaving as expected. The life cycle of the active length of these sensors according to the manufacturer is more than a million cycles [3]. Therefore, to help improve the durability of the sensors, the base of it (the fragile part) will have to be supported with a sturdier material to ensure that it operates as expected.

To get the readings from all the sensors across the tether, microcontrollers will need to be placed along its length. If six sensors are required per sensing point, the microcontroller must have six analogue inputs while also being small in size. After reviewing the current commercially viable microcontrollers, a number of suitable microcontrollers were identified; the ATtiny85 which has 3 analogue inputs or the ATtiny26 which has 6 analogue inputs. These microcontrollers will require some power to operate and this needs to be considered when choosing the appropriate power supply and whether it will be possible to power all of them simultaneously along the tether.

The following equation can be used to calculate the power consumption of all the components along the tether:

$$power = (P_m + 6 \cdot P_s)N \quad (4.19)$$

Where P_m is the power consumption of the micro controller (5 mW for ATtiny26), P_s is the power consumption of the flex sensors (approximately 0.6 mW, it is multiplied by 6 as 6 sensors are required for a 3D tether localisation system) and N is the number of nodes along the tether. If a 30 m tether is sampled every 0.1 m, the power consumption of such a system will be approximately 2.58 W, which will not be an issue.

Furthermore, the extra components and wires on the tether will increase the weight of the tether and hence it might affect the movement of the robot. Therefore, careful consideration has to be made in order to make sure that the cable is neutrally buoyant after all of this added mass. Moreover, the sensors and circuitry needs to be water proofed properly.

The microcontrollers must send the data along the tether, if the communication protocol that will be used is I2C, the base station (computer that will receive and process the data) will be used as the master and all the other microcontrollers will be the slaves. However, I2C will be difficult to use due to the long bus length (which could be increased by choosing corresponding pull-up resistors). For example a 10 m cable limits the baud rate to 10Kbaud². Increasing the length of the tether to a more practical length, like 30 m will further decrease this baud rate and therefore make the use of I2C impractical (even though I2C extenders can be used to increase the bus length). On the other hand a CAN bus can also be used to retrieve the data from the sensors.

²<http://www.mosaic-industries.com/embedded-systems/sbc-single-board-computers/freescale-hcs12-9s12-c-language/instrument-control/i2c-bus-specifications>

The separation between sensors cause an inaccuracy in the estimated end position and when expanding this system to a much longer tether, these errors will add up significantly. Furthermore, the length of the sensor separations will greatly effect the accuracy of the system. Moreover, if one sensor fails along the tether, it will be really difficult to account for and hence the accuracy of the system will be further affected.

Due to all the mentioned challenges with the system, it is not recommended to further investigate this solution.

4.5 Summary

In this chapter the need for a 2D localisation system before a 3D one was discussed. The suggested localisation method required sensors to measure characteristics along the tether in order to estimate the end position of the tether, therefore the possible sensors were discussed and one was chosen to be used.

Knowing how the sensor works and a few assumptions to simplify the problem, it was possible to come up with an algorithm to estimate the end position of the tether. The uncertainty of the sensor readings was $\pm 3.10^\circ$ which means that for a 30 m tether deployed along the y-axis on a 2D plane the average absolute error in the estimated position was (2.79,0.01) m, and the uncertainty in the estimated position was $\pm(3.00,9.68)$ m. Furthermore, it was discovered that to provide a precise and accurate estimation of the end position of a 30 m tether, the measured angle must have a precision of $\pm 0.02^\circ$. This implies that expanding this system is unfeasible. Another problem with the system is if one sensor no longer functions, the error in the estimated end position will drastically increase.

Four methods were considered to estimate the behaviour of the tether in the sections without a sensor, two of which provided accurate results for different experiments. These assumptions provided an error in the estimated final position. The errors were analysed and it was evident that for one sensor, the error in the estimated final position is relatively low, however as the system is expanded, the error propagates throughout the system causing a large uncertainty and error in the final estimated position.

Finally, the issues that were experienced with the test rig and the localisation model were discussed and the possible solutions to them were explained. It was concluded that this method should no longer be considered and researched due to the build up of error throughout the system and the many issues that will come up when expanding the system to a longer tether.

Chapter 5

Camera Tether Localisation System

In Chapter 4 it was concluded that a tether localisation system that uses sensors attached along the tether has many challenges and a large error accumulation which make the system unusable. Therefore, another method for localising the tether needs to be considered. This chapter explores the possibility of using a visual localisation system that uses nodes with cameras and a distinct LED colour/formation placed along the tether. Figure 5.1 shows a prototype of the node design, where the circuitry will be inside of the enclosure.

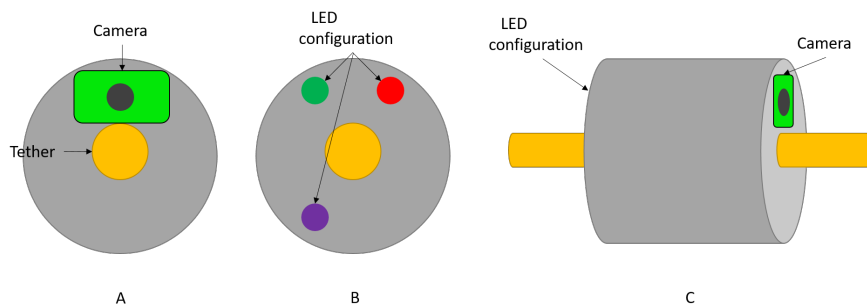


Figure 5.1: Prototype for the node design. A shows the front side of the node with the camera. B shows the back side of the node with the LED markers. C shows the side view of the enclosure of the node placed along the tether.

The system would allow for one camera to find and localise the next node in the series. The separation distance between the nodes will be the main factor that affects the practicality of the system in the target environment mentioned in Chapter 1. A further advantage of this localisation system is its low cost. The components included in one node can be bought individually for a total of £40. This cost is significantly lower

than other tether localisation systems and this cost could be reduced even further when components for multiple nodes are bought in bulk. Depending on the visibility in the water and the accuracy required the distance between each node would vary.

The starting (first) node can localise the position of the following node by knowing which LED formation/colours to look for. Then that node would look for the next and so on. By knowing the position of node 2 relative to node 1, and by knowing the position of node 3 relative to node 2, it is possible to infer the position of node 3 relative to node 1 similarly to Section 4.2. Then the position of the robot relative to the starting node can be inferred. This approach will be usable in dark/turbid water by placing the nodes at a distance where the water would not affect the visibility of the next node.

As this system uses visual localisation, issues arise when any of the cameras lose line of sight of their corresponding node, this could be due to a hardware failure or an obstacle blocking the node. This issue can be resolved by allowing each camera to search for the LEDs of the next 4 nodes, increasing the robustness of the system. If node 2 can localise node 4 but cannot localise node 3 it assumes that node 3 is either behind an obstacle as it is not visible or that it is faulty and no longer functioning correctly and therefore ignores node 3 from the chain. Even though, node 3 may very well be functioning correctly and can localise node 4 with respect to itself but since node 2 cannot localise node 3, it must be ignored from the chain and the end point must be estimated without using node 3. This same concept can be applied if more than one point cannot be seen, as long as the chain can continue there should be no issues with localising the end point of the tether.

Although the robustness of this system can be increased, this system still has an issue where if one node can no longer find any points that it is expecting, which means either the other nodes are no longer functioning or the robot/tether has went around a wall or obstacle which no longer allows the following nodes to be seen. Therefore, the chain can no longer be continued and hence the position of the end point cannot be estimated. Figure 5.2 shows an example of how this problem might occur inside the environment.

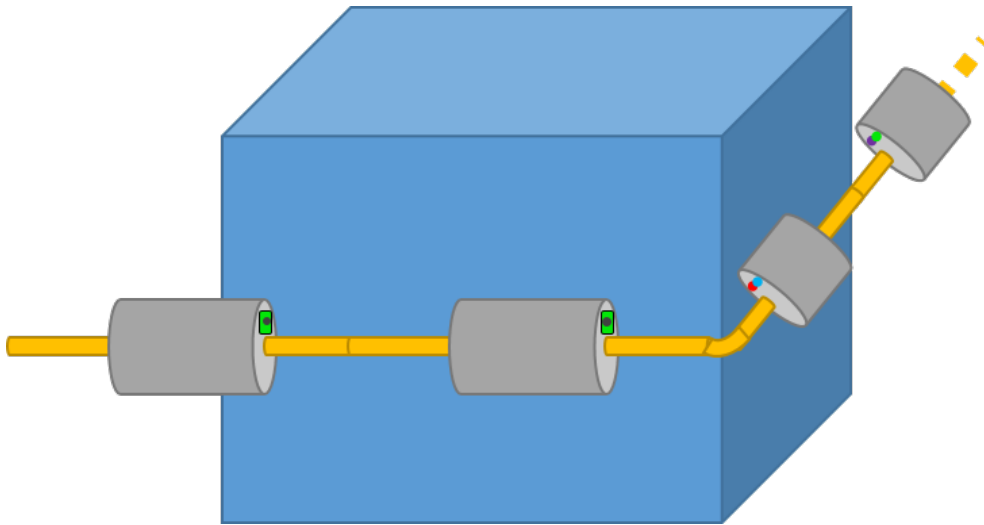


Figure 5.2: Illustration of the corner problem where one node can no longer localise any further nodes due to a wall or an obstacle.

Here lies an interesting problem, where one solution could be to increase the number of nodes to reduce the chance of the tether being hidden. This comes at the cost of electrical power (to power all the single board computers (like raspberry pi zero w which would be suitable for testing the system), LEDs and cameras), computational power required to do all the calculation and adding more weight to the tether.

The other and better solution to when this problem happens is to have the last node that can be localised run a visual inspection algorithm to search for the tether (yellow sheath), which should be distinct in the environment. If it can see and identify the tether it can estimate from its shape and its known length, the approximate location of the next node. Since the following nodes (the ones around the wall/obstacle) are still functioning, it is possible to continue estimating the position of the robot the same as before. This of course provides a higher uncertainty in the estimated position of the robot however it will always provide an approximate position of the robot.

5.1 Challenges With Proposed System

The proposed method provides a solution which should provide an accurate estimate of the position of the robot. However, the system has some challenges that are unique to it and some of which are similar to the flex sensor method. These challenges will be discussed in this section however, the general challenges of visual localisation systems were not included since they were mentioned in Chapter 2.

The power draw required to power all the components (raspberry pi zero or whatever is used to process the camera data, camera and LEDs) would be considerable since there will be multiple of them along the tether. The following equation can be used to calculate the power consumption of all the components along the tether:

$$pow = (P_p + P_c + 3P_L)N_n \quad (5.1)$$

Where P_p is the power consumption of the single board computer, P_c is the power consumption of the camera, P_L is the power consumption of the LEDs which is multiplied by 3 since there are 3 LEDs in the configuration and N_n is the number of nodes along the tether. If a Raspberry Pi zero and camera are used, they have a power consumption of 0.85 W and 1.25 W respectively. LEDs can consume around 0.075 W each. Assuming that a 30 m tether is used and there is a node per meter, the number of nodes will be 30. Using equation 5.1, the power consumption of such a system will be approximately 70 W. Powering all of these components along with powering the robot will require a sufficient power supply and good power management along the tether to ensure that all the nodes can operate simultaneously. The number of nodes required will be dependant on the clarity of the water in the environment.

Extra weight will be added to the tether as each one will require a single board computer, camera and three LEDs. This added weight to the tether could cause an issue by effecting the buoyancy of tether and thus it would affect the movements of the underwater vehicle. However, this could be taken into account when designing the tether and using material that could help with ensuring that the tether remains neutrally buoyant after the addition of the nodes. Additionally, the nodes will be larger than the tether, which will increase its size.

This method requires the cameras to be calibrated for the LED configurations,

which will be difficult since access to the working environment is very difficult. However, if it is possible to get the characteristics of the water in the target environment, it might be possible to calibrate them outside and assume that they will provide similar performance in said environment.

Similar to the previous system, I2C will be difficult to use due to the bus length and therefore an I2C bus extender will have to be used if I2C is the chosen communication protocol. I2C can be used in this methods, as not as much data needs to be transferred along the bus, since less sensors are required. Additionally, like the previous method the CAN bus protocol can be used.

5.2 Summary

In this chapter a visual tether localisation method was discussed. The suggested localisation method uses cameras and LED unique identifiers along the tether to estimate the end position of the tether. This localisation system requires much more computational power compared to the localisation system mentioned in Chapter 4, but it requires less nodes along the tether. This means that a prototype will be easier to implement and test. Since this system is a visual localisation system, there are problems when a camera can no longer locate any of the following markers. To overcome this problem a few solutions are suggested.

The issues that could occur with the system were discussed. It was concluded that this localisation system is worth investigating further to verify its accuracy and precision.

Chapter 6

Conclusion and Future Work

This thesis has focused on two different aspects which are a tether localisation system and a tether model. In order to explain the requirement of a tether localisation system the current underwater localisation systems were reviewed and discussed. Additionally, tether localisation systems were summarised and discussed to explain why they are not viable to be used in the target environment.

Two tether localisation systems were considered, one using flex sensors and one using an image based localisation system.

The flex sensor approach used sensors to measure characteristics along the tether in order to estimate the position of the end point of the tether. The other possible sensors were also discussed. Knowing how the sensor works and a few assumptions to simplify the problem, it was possible to come up with an algorithm to estimate the end position of the tether. However, while the problem was theoretically possible it has too many issues to be expanded and researched further. Additionally, the uncertainty of the sensor readings was $\pm 3.10^\circ$ which means that for a 30 m tether deployed along the y-axis on a 2D plane the average absolute error in the estimated position was (2.79,0.01) m, and the uncertainty in the estimated position was $\pm(3.00,9.68)$ m. These errors imply that expanding this system is unfeasible. Another problem with the system is if one sensor no longer functions, the error in the estimated end position will drastically increase. Furthermore, the error due to the sensor separation propagates throughout the system causing a large error and uncertainty in the estimated position of the end point of the tether.

As the tether localisation system that uses flex sensors was considered to be impractical another tether localisation system was thought of and explained. The system uses an image based localisation system to estimate the end position of the tether. Even though the system is a visual localisation system it should provide accurate data in the target environment due to the short distances that it has to work at. However, it also has some downfalls that make expanding the system difficult.

A 2D dynamics tether model was researched and modified in order to estimate the effect of the tether on the robot and also to estimate the behaviour of the tether for different robotic movements. Some experimental data was compared to the results obtained from the model to validate its solutions. The model was then adapted in order to allow it to simulate the tether moving as if a robot is pulling its end point along the plane. This simulation provided a result which visually looks to be correct but has not been validated in order to see how accurate it is compared to a real world example. The model used is not complete and still requires work in order for it to accurately estimate the tether's behaviour and the effects of the forces of the tether on the robot's movements.

In summary, tether localization using flex sensors is infeasible due to their low accuracy. The error propagation along a 30 m tether suggests that the target accuracy of the sensors along the tether should be $\pm 0.02^\circ$. A vision-based system was also considered, however the system has similar implementation challenges. Therefore, it appears as if FBG sensors may be the only viable solution longer-term, however more research is required on the technology to test its capabilities.

6.1 Future Work

The further work for the tether model was discussed in Chapter 3.

The implementation of a 2D localisation system using flex sensors was found to be unfeasible. Further to this, the system was determined to lack the accuracy required of a tether localisation system. Therefore, further work should not focus on the development of a localisation system using flex sensors.

A theoretical solution for an image based localisation system was proposed in Chapter 5. A verification of this system using a few nodes could be pursued to verify

the accuracy and precision of the system. However, as mentioned in Chapter 5 the system has many challenges to overcome before it is viable to use along a 30 m tether.

Since the both aforementioned tether localisation systems have many challenges, investing in the FBG solution would allow for the opportunity to test the systems capabilities and limitations. From the technology review conducted in Chapter 2, the FBG system can provide mm accuracy in the estimated end position which would meet the requirements mentioned in Chapter 2.

Appendix A

Work done on the AVEXIS™

A.1 Variable Speed Control

The AVEXIS™ had simple motor control where the motors would operate at full speed or they would be off. This method doesn't allow for fine tuning of the position of the robot when it is controlled. So to implement a simple control system on the robot, the first task was to redesign the PCB and implement variable speed control for each motor.

Before printing and populating the entire PCB for variable speed control a small test board (seen in figure A.1) was designed to ensure that the circuit is functional and behaves in the expected manner. This was done to cut costs on the components and manufacturing the full PCB in case the circuit did not work as expected.

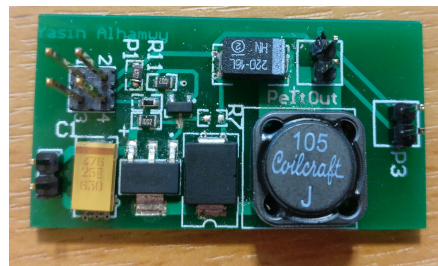


Figure A.1: Test PCB designed for variable speed control

When the behaviour of the circuit was verified, the main board was printed, populated (shown in Figure A.2) and then tested.

A new program had to be written as the previous one does not take into consideration any variable speed control. After the code was written it was tested to see if the AVEXIS™ now moves at different speeds. Two tests were conducted to see if the pumps were working at a variable speed, one of which was a bench-top test where the

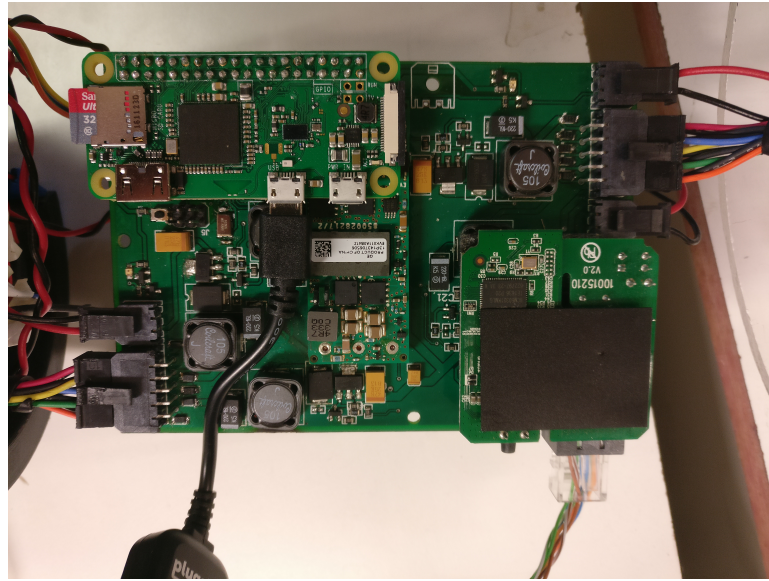


Figure A.2: Image of the front side of the variable speed control PCB

voltage was measured across the pumps terminals as the user changed the PWM signal's duty cycle (done using a 2-axis controller). The other test was a visual one where the AVEXISTM was placed in a water tank and manoeuvred around.

A.2 Depth Hold

The AVEXISTM had no autonomous control. Therefore, to add a level of autonomy to the robot a depth hold controller was implemented. A simple proportional integral derivative (PID) controller was implemented on the Arduino. The depth reading is obtained by the MS5837-30BA pressure sensor, this reading is read by the Raspberry Pi using the I²C interface and then passed on to the Arduino over the serial interface. The Arduino then reads the data from the Raspberry Pi and calculates the required control action to keep the AVEXISTM at the required depth that the user specifies when starting the system.

Currently the AVEXISTM oscillates around the desired point by approximately ± 4 cm if the depth reading is read at 4 significant figures (as seen in Figure A.4) and ± 3 cm if the depth reading is read at 2 significant figures (as seen in Figure A.5). These oscillations can be reduced by further tuning of the PID parameters. Figure A.3 shows a snapshot of the AVEXISTM maintaining its depth with a link to a video.



Figure A.3: Snapshot of AVEXISTM from video showing its depth hold capabilities (video available at <https://youtu.be/bEK0zR1iH-E>)

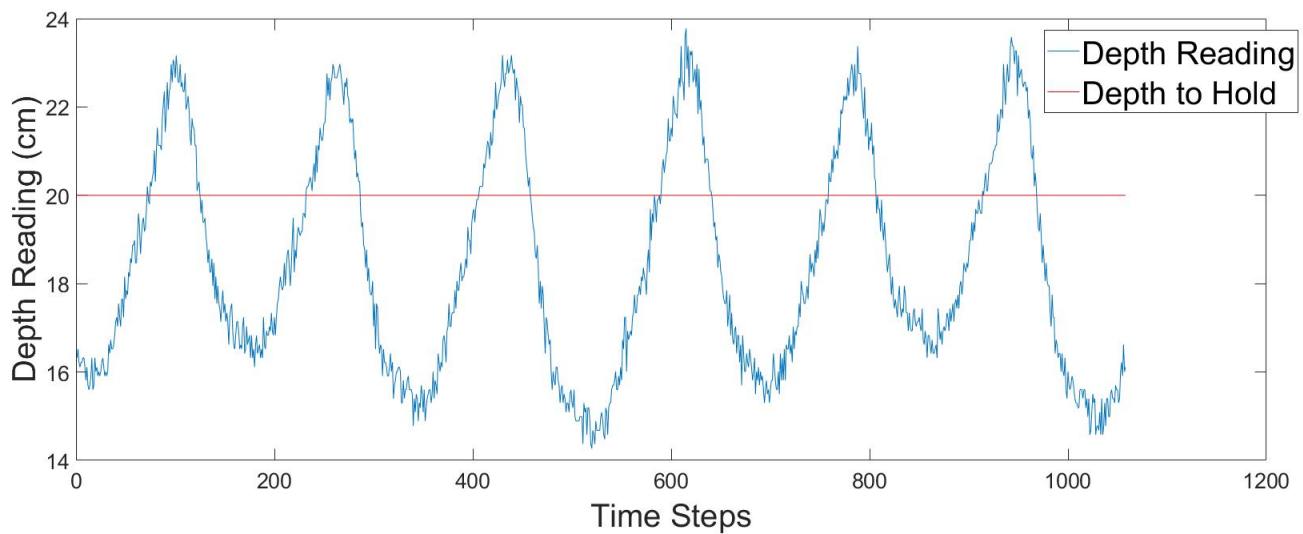


Figure A.4: Data from the AVEXISTM while maintaining a depth of 20 cm. The data retrieved from the sensor was read to 4 significant figures.

To validate that the AVEXISTM was approximately floating around the required depth, a meter rule was used to mark the depth of the water. The sensor was not calibrated before use and hence the depth measured was approximately 10 cm away from the actual depth of the AVEXISTM, and therefore the AVEXISTM was holding depth at a point that was approximately 10 cm away from the desired depth. In order to calibrate the sensor and get accurate readings a test rig has to be used.

Figure A.6 shows a sketch of the proposed calibration test rig that might be used.

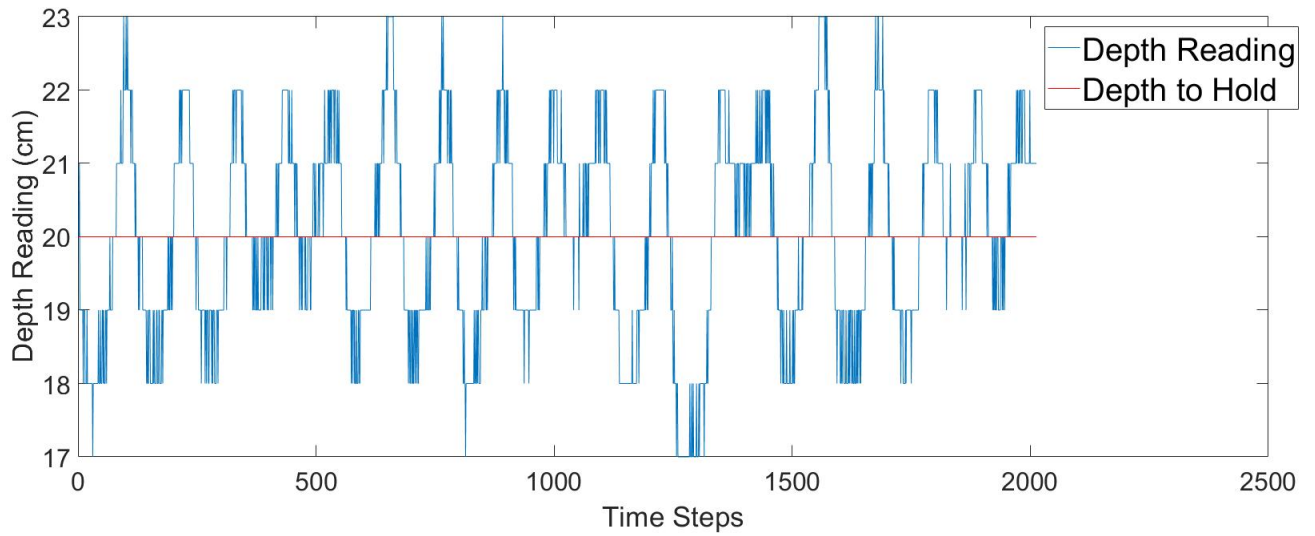


Figure A.5: Data from the AVEXIS™ while maintaining a depth of 20 cm. The data retrieved from the sensor was read to 2 significant figures.

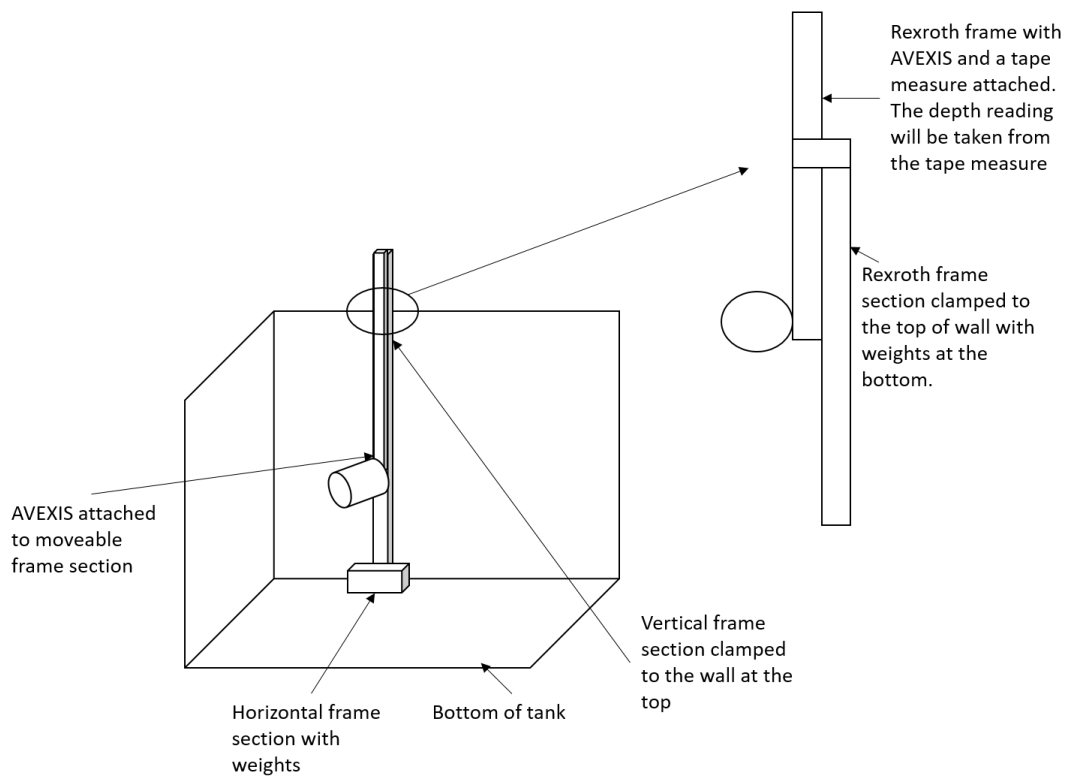


Figure A.6: Test rig designed to calibrate the pressure sensor to provide accurate depth readings

The idea is to have a Rexroth frame clamped to the top of tank and another moveable Rexroth frame which has the AVEXIS™ attached to it. The moveable frame will have a tape measure attached to it so that the depth of the AVEXIS™ can be measured and then the sensor can be calibrated.

A.3 Thrust Allocation of Actuators

A previous conference paper started by a Postdoctoral researcher has yet to be finished as it requires experimental and simulation results. The first step of carrying on with his work was to implement variable speed control on the AVEXIS™ which was completed. The second step was to set up the thrust allocation matrix for the AVEXIS™. In order to do this the forces generated by the pumps need to be measured. These measurements were taken by the FC22 compression load cell. Figures A.7 and A.8 show the results obtained from the load where each dot indicates the average force from 50 measurements at the corresponding duty cycle. As seen from the graphs the error bars are quite large, this is due to the sensitivity of the FC22 compression load cell. Since the force generated by the pump is small, the readings are effected by noise. One way of reducing the error is to use a load cell with much higher sensitivity to get better readings of the small force generated by the pumps.

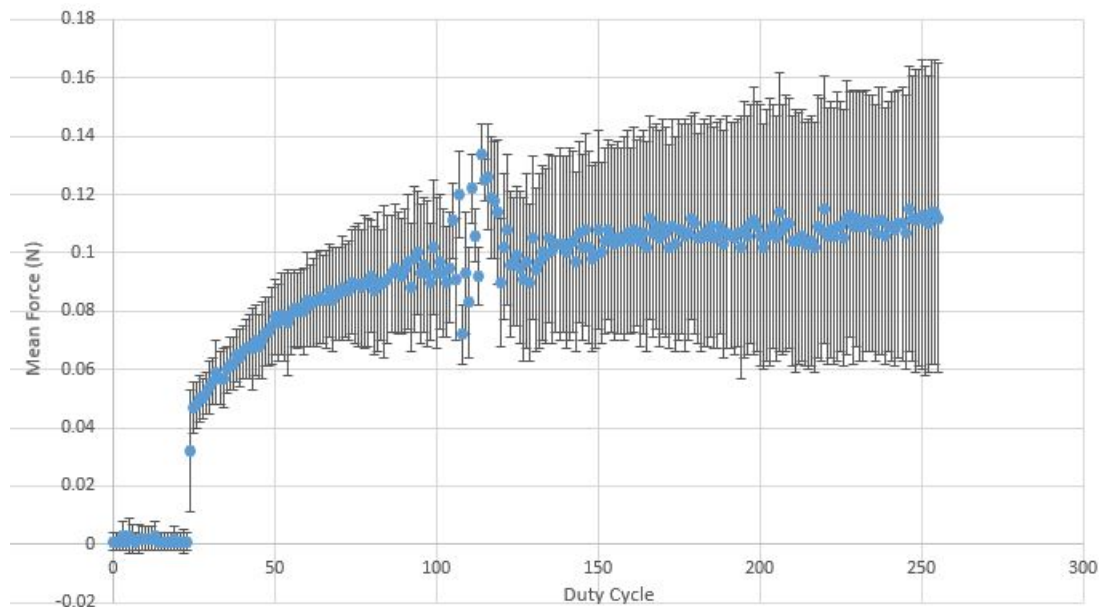


Figure A.7: PWM to force allocation when the motor is ramping up from 0% duty cycle to 100%.

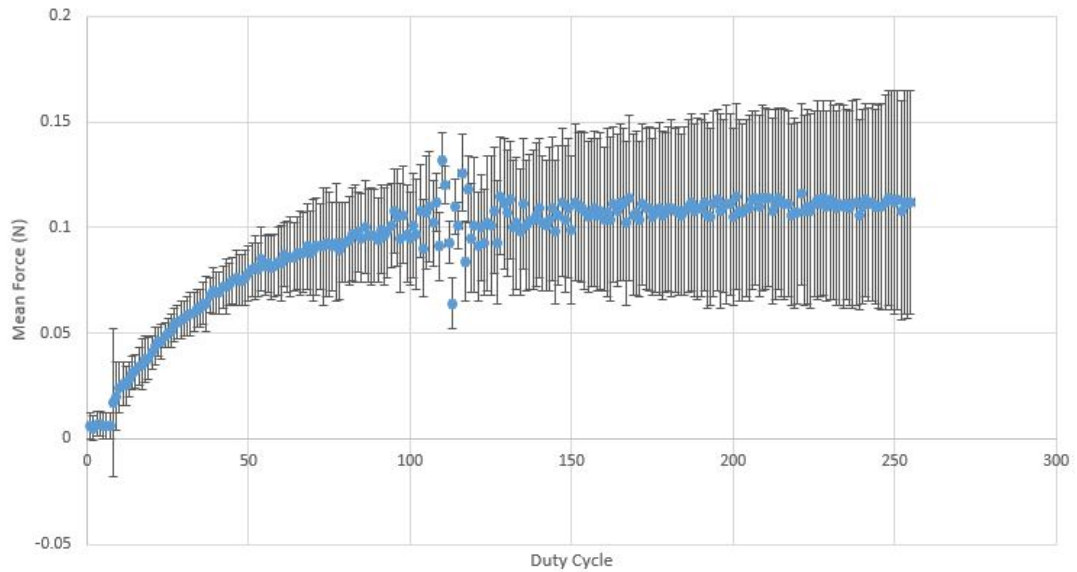


Figure A.8: PWM to force allocation when the motor is ramping down from 100% duty cycle to 0%.

From these results it is possible to determine the thrust required given the desired forces from the controller and hence an experiment can be conducted to complete the conference paper.

Another Postdoctoral researcher is currently working on developing a visual localisation system. Once the system can localise the AVEXISTM a trajectory tracking controller will be implemented on the AVEXISTM to get it to move to desired locations without any manual control.

Bibliography

- [1] “Fukushima disaster: Robot finds possible melted nuclear fuel - BBC News.”
- [2] P. McGarey, K. MacTavish, F. Pomerleau, and T. D. Barfoot, “TSLAM: Tethered simultaneous localization and mapping for mobile robots,” *The International Journal of Robotics Research*, vol. 36, pp. 1363–1386, oct 2017.
- [3] Spectra Symbol, “Flex Sensor,” tech. rep.
- [4] L. T. Rauchenstein, A. Vishnu, X. Li, and Z. D. Deng, “Improving underwater localization accuracy with machine learning,” *The Journal of the Acoustical Society of America*, vol. 143, p. 74902, 2018.
- [5] Yunfeng Han, Cuie Zheng, and Dajun Sun, “Accurate underwater localization using LBL positioning system,” *OCEANS 2015 - MTS/IEEE Washington*, pp. 1–4, 2017.
- [6] H.-P. Tan, W. K. G. Seah, M. Waldmeyer, and R. Diamant, “A Survey of Techniques and Challenges in Underwater Localization,” vol. 38, no. 14, pp. 1663–1676, 2011.
- [7] I. F. Akyildiz, D. Pompili, and T. Melodia, “Underwater acoustic sensor networks: research challenges,” 2005.
- [8] A. Dikarev, A. Griffiths, S. A. Watson, B. Lennox, and P. R. Green, “Combined multiuser acoustic communication and localisation system for μ AUVs operating in confined underwater environments,” *IFAC-PapersOnLine*, vol. 28, pp. 161–166, may 2015.
- [9] C. Wong, E. Yang, X.-T. Yan, and D. Gu, “Autonomous robots for harsh environments: a holistic overview of current solutions and ongoing challenges,” *SYSTEMS SCIENCE & CONTROL ENGINEERING: AN OPEN ACCESS JOURNAL*, vol. 6, no. 1, pp. 213–219, 2018.

- [10] A. Poncela, C. Urdiales, B. Fernández-Espejo, and F. Sandoval, “Place characterization for navigation via behaviour merging for an autonomous mobile robot,” in *Proceedings of the Mediterranean Electrotechnical Conference - MELECON*, pp. 350–355, 2008.
- [11] S. Goswami, *Indoor location technologies*. Springer New York, jan 2013.
- [12] H. Zender, O. Martínez Mozos, P. Jensfelt, G. J. Kruijff, and W. Burgard, “Conceptual spatial representations for indoor mobile robots,” *Robotics and Autonomous Systems*, vol. 56, pp. 493–502, jun 2008.
- [13] G. Balamurugan, J. Valarmathi, and V. P. Naidu, “Survey on UAV navigation in GPS denied environments,” *International Conference on Signal Processing, Communication, Power and Embedded System, SCOPES 2016 - Proceedings*, no. October 2018, pp. 198–204, 2017.
- [14] K. Vickery, “Acoustic positioning systems - a practical overview of current systems,” *Proceedings of the IEEE Symposium on Autonomous Underwater Vehicle Technology*, pp. 5–17, 1998.
- [15] M. Nancekievill, J. Espinosa, S. Watson, B. Lennox, A. Jones, M. J. Joyce, J. I. Katakura, K. Okumura, S. Kamada, M. Katoh, and K. Nishimura, “Detection of simulated fukushima daichii fuel debris using a remotely operated vehicle at the naraha test facility,” *Sensors (Switzerland)*, vol. 19, no. 20, pp. 1–16, 2019.
- [16] J. Horgan, D. Toal, P. Ridao, and R. Garcia, “REAL-TIME VISION BASED AUV NAVIGATION SYSTEM USING A COMPLEMENTARY SENSOR SUITE,” tech. rep., 2007.
- [17] D. Ribas, P. Ridao, J. D. Tardós, and J. Neira, “Underwater SLAM in man-made structured environments,” *Journal of Field Robotics*, vol. 25, no. 11-12, pp. 898–921, 2008.
- [18] J. Bao, D. Li, X. Qiao, and T. Rauschenbach, “Integrated navigation for autonomous underwater vehicles in aquaculture: A review,” 2019.
- [19] H. Li, Y. He, X. Cheng, H. Zhu, and L. Sun, “Security and privacy in localization for underwater sensor networks,” *IEEE Communications Magazine*, vol. 53, pp. 56–62, nov 2015.

- [20] G. Tuna and V. C. Gungor, "A survey on deployment techniques, localization algorithms, and research challenges for underwater acoustic sensor networks," *International Journal of Communication Systems*, vol. 30, p. e3350, nov 2017.
- [21] I. Tsitsimpelis, C. J. Taylor, B. Lennox, and M. J. Joyce, "A review of ground-based robotic systems for the characterization of nuclear environments," 2019.
- [22] J. B. Matthews and I. A. Nesnas, "On the design of the Axel and DuAxel rovers for extreme terrain exploration," *IEEE Aerospace Conference Proceedings*, pp. 1–10, 2012.
- [23] S. Ali Ajwad and J. Iqbal, "RECENT ADVANCES AND APPLICATIONS OF TETHERED ROBOTIC SYSTEMS," *Sci.Int.(Lahore)*, vol. 26, no. 5, pp. 2045–2051, 2014.
- [24] N. Michael, S. Shen, K. Mohta, Y. Mulgaonkar, V. Kumar, K. Nagatani, Y. Okada, S. Kiribayashi, K. Otake, K. Yoshida, K. Ohno, E. Takeuchi, and S. Tadokoro, "Collaborative mapping of an earthquake-damaged building via ground and aerial robots," *Journal of Field Robotics*, vol. 29, pp. 832–841, sep 2012.
- [25] P. M. Mcgarey, *Towards Autonomy and Mobility for a Tethered Robot Exploring Extremely Steep Terrain*. PhD thesis, 2017.
- [26] A. Griffiths, A. Dikarev, P. R. Green, B. Lennox, X. Poteau, and S. Watson, "AVEXIS-Aqua Vehicle Explorer for In-Situ Sensing," *IEEE Robotics and Automation Letters*, vol. 1, no. 1, pp. 282–287, 2016.
- [27] S. S. D. C. Botelho, P. Drews, G. L. Oliveira, and M. D. S. Figueiredo, "Visual odometry and mapping for underwater autonomous vehicles," in *2009 6th Latin American Robotics Symposium, LARS 2009*, 2009.
- [28] D. Scaramuzza and F. Fraundorfer, "Tutorial: Visual odometry," *IEEE Robotics and Automation Magazine*, vol. 18, pp. 80–92, dec 2011.
- [29] K. Nirmal, A. G. Sreejith, J. Mathew, M. Sarpotdar, A. Suresh, A. Prakash, M. Safonova, and J. Murthy, "Noise modeling and analysis of an IMU-based attitude sensor: improvement of performance by filtering and sensor fusion," in *Advances in Optical and Mechanical Technologies for Telescopes and Instrumentation II*, vol. 9912, p. 99126W, SPIE, jul 2016.

- [30] N. H. Kussat, C. D. Chadwell, and R. Zimmerman, "Absolute positioning of an autonomous underwater vehicle using GPS and acoustic measurements," *IEEE Journal of Oceanic Engineering*, vol. 30, no. 1, pp. 153–164, 2005.
- [31] A. Vasilijevic, B. Borovic, and Z. Vukic, "Underwater vehicle localization with complementary filter: Performance analysis in the shallow water environment," *Journal of Intelligent and Robotic Systems: Theory and Applications*, vol. 68, no. 3-4, pp. 373–386, 2012.
- [32] F. Ijaz, H. K. Yang, A. W. Ahmad, and C. Lee, "Indoor positioning: A review of indoor ultrasonic positioning systems," *International Conference on Advanced Communication Technology, ICACT*, pp. 1146–1150, 2013.
- [33] K. Vickery, "Acoustic positioning systems - new concepts: The future," in *Proceedings of the IEEE Symposium on Autonomous Underwater Vehicle Technology*, pp. 103–110, IEEE, 1998.
- [34] J. Peng, M. E. El Najjar, C. Cappelle, D. Pomorski, F. Charpillet, and A. Deeb, "A novel geo-localisation method using GPS, 3D-GIS and Laser scanner for intelligent vehicle navigation in urban areas," *2009 International Conference on Advanced Robotics, ICAR 2009*, 2009.
- [35] C. Cappelle, M. E. B. El Najjar, D. Pomorski, and F. Charpillet, "Localisation in urban environment using GPS and INS aided by monocular vision system and 3D geographical model," in *IEEE Intelligent Vehicles Symposium, Proceedings*, pp. 811–816, 2007.
- [36] E. Dalberg, A. Lauberts, R. K. Lennartsson, M. J. Levonen, and L. Persson, "Underwater target tracking by means of acoustic and electromagnetic data fusion," in *2006 9th International Conference on Information Fusion, FUSION*, 2006.
- [37] D. A. Duecker, A. R. Geist, M. Hengeler, E. Kreuzer, M. A. Pick, V. Rausch, and E. Solowjow, "Embedded spherical localization for micro underwater vehicles based on attenuation of electro-magnetic carrier signals," *Sensors (Switzerland)*, vol. 17, no. 5, 2017.
- [38] Y. Hada and K. Takase, "Multiple mobile robot navigation using the indoor global positioning system (iGPS)," in *IEEE International Conference on Intelligent Robots and Systems*, vol. 2, pp. 1005–1010, 2001.

- [39] J. Yan, C. C. Tiberius, G. J. Janssen, P. J. Teunissen, and G. Bellusci, "Review of range-based positioning algorithms," *IEEE Aerospace and Electronic Systems Magazine*, vol. 28, no. 8 PART 2, pp. 2–27, 2013.
- [40] E. Rowan, "LBL underwater positioning," *Hydro International*, vol. 12, no. 1, 2008.
- [41] G. C. Messenger and M. S. Ash, *The effects of radiation on electronic systems*. Van Nostrand Reinhold Co, 1986.
- [42] P. E. Dodd, M. R. Shaneyfelt, J. R. Schwank, and J. A. Felix, "Current and future challenges in radiation effects on CMOS electronics," in *IEEE Transactions on Nuclear Science*, vol. 57, pp. 1747–1763, aug 2010.
- [43] M. J. Nancekievill, "The Radiation Tolerance and Development of Robotic Platforms for Nuclear Decommissioning," 2017.
- [44] J. Medard, "USBL in dam survey by ROV," *Hydro International*, vol. 10, no. 8, pp. 19–21, 2008.
- [45] D. Thomson and I. Product, "Acoustic Positioning Systems," 2005.
- [46] E. M. L.J, "Underwater Localisation Systems for Exploration of Hazardous Environments," 2018.
- [47] X. Che, I. Wells, G. Dickers, P. Kear, and X. Gong, "Re-Evaluation of RF Electromagnetic Communication in Underwater Sensor Networks," tech. rep., 2010.
- [48] D. Park, K. Kwak, J. Kim, and W. K. Chung, "Underwater sensor network using received signal strength of electromagnetic waves," in *IEEE International Conference on Intelligent Robots and Systems*, vol. 2015-Decem, pp. 1052–1057, Institute of Electrical and Electronics Engineers Inc., dec 2015.
- [49] D. Park, K. Kwak, W. K. Chung, and J. Kim, "Development of Underwater Short-Range Sensor Using Electromagnetic Wave Attenuation," *IEEE Journal of Oceanic Engineering*, vol. 41, pp. 318–325, apr 2016.
- [50] F. Bonin-Font, A. Ortiz, and G. Oliver, "Visual navigation for mobile robots: A survey," *Journal of Intelligent and Robotic Systems: Theory and Applications*, vol. 53, pp. 263–296, nov 2008.

- [51] R. Giubilato, M. Pertile, and S. Debei, "A comparison of monocular and stereo visual FastSLAM implementations," in *3rd IEEE International Workshop on Metrology for Aerospace, MetroAeroSpace 2016 - Proceedings*, pp. 227–232, Institute of Electrical and Electronics Engineers Inc., sep 2016.
- [52] T. Bailey and H. Durrant-Whyte, "Simultaneous localization and mapping (SLAM): Part II," *IEEE Robotics and Automation Magazine*, vol. 13, pp. 108–117, sep 2006.
- [53] R. Mur-Artal, J. M. Montiel, and J. D. Tardos, "ORB-SLAM: A Versatile and Accurate Monocular SLAM System," *IEEE Transactions on Robotics*, vol. 31, pp. 1147–1163, oct 2015.
- [54] C. Chen, H. Zhu, M. Li, and S. You, "A review of visual-inertial simultaneous localization and mapping from filtering-based and optimization-based perspectives," *Robotics*, vol. 7, no. 3, pp. 1–20, 2018.
- [55] D. T. Savaria and R. Balasubramanian, "V-SLAM: Vision-based simultaneous localization and map building for an autonomous mobile robot," in *IEEE International Conference on Multisensor Fusion and Integration for Intelligent Systems*, pp. 1–6, 2010.
- [56] D. Forouher, J. Hartmann, M. Litza, and E. Maehle, "Sonar-based FastSLAM in an underwater environment using walls as features," in *IEEE 15th International Conference on Advanced Robotics: New Boundaries for Robotics, ICAR 2011*, pp. 588–593, 2011.
- [57] J. J. Leonard and H. F. Durrant-Whyte, *Directed Sonar Sensing for Mobile Robot Navigation*. 1992.
- [58] S. B. Williams, P. Newman, G. Dissanayake, and H. Durrant-Whyte, "Autonomous underwater simultaneous localisation and map building," in *Proceedings - IEEE International Conference on Robotics and Automation*, vol. 2, pp. 1793–1798, 2000.
- [59] D. Ribas, P. Ridao, J. Neira, and J. D. Tardós, "SLAM using an imaging sonar for partially structured underwater environments," in *IEEE International Conference on Intelligent Robots and Systems*, pp. 5040–5045, 2006.

- [60] H. Alismail, L. D. Baker, and B. Browning, “Continuous Trajectory estimation for 3D SLAM from actuated lidar,” in *Proceedings - IEEE International Conference on Robotics and Automation*, pp. 6096–6101, Institute of Electrical and Electronics Engineers Inc., sep 2014.
- [61] D. McLeod, J. Jacobson, M. Hardy, and C. Embry, “Autonomous Inspection using an Underwater 3D LiDAR,” *OCEANS - San Diego*, 2013.
- [62] S. Huang and G. Dissanayake, “Robot Localization: An Introduction,” *Wiley Encyclopedia of Electrical and Electronics Engineering*, pp. 1–10, 2016.
- [63] “Jackal UGV - Small Weatherproof Robot - Clearpath.”
- [64] “Phantom 4 RTK - Next Gen Mapping Solution - DJI.”
- [65] Iaea, “Use of nuclear material accounting and control for nuclear security at facilities,” tech. rep.
- [66] “International Atomic Energy Agency — Atoms for Peace and Development, <https://www.iaea.org/>.”
- [67] J. Dean, “A UK comparison for measurements of low levels of gamma-emitters in waste drums,” *Applied Radiation and Isotopes*, vol. 67, pp. 678–682, may 2009.
- [68] “Direct Scientific - Decay Drums for Radioactive Waste.”
- [69] “Argonne national Laboratory - Nuclear Fuel,” tech. rep.
- [70] X. Xiao, Y. Fan, J. Dufek, and R. Murphy, “Indoor UAV Localization Using a Tether,” *2018 IEEE International Symposium on Safety, Security, and Rescue Robotics, SSRR 2018*, pp. 1–6, 2018.
- [71] Jeremy E. Frank, Richard Geiger, David R. Kraige, and Arun Murali, “Smart tether system for underwater navigation and cable shape measurement,” jan 2008.
- [72] Luna, “Fiber Optic Shape Sensing — 2 Technology Snapshot,” tech. rep., 2013.
- [73] NASA, “Highly Accurate Position Detection and Shape Sensing with Fiber Optics,” tech. rep.
- [74] “Fiber Gratings: Basic Theory and Sensing Principle,” tech. rep.

- [75] R. J. Roesthuis, S. Janssen, and S. Misra, “On using an array of fiber Bragg grating sensors for closed-loop control of flexible minimally invasive surgical instruments,” in *IEEE International Conference on Intelligent Robots and Systems*, pp. 2545–2551, IEEE, nov 2013.
- [76] “Velodyne LiDAR PUCK,” tech. rep.
- [77] B. Siciliano and O. Khatib, *Springer Handbook of Robotics*. Springer Berlin Heidelberg, 2008.
- [78] C. West, F. Arvin, W. Cheah, A. West, S. Watson, M. Giuliani, and B. Lennox, “A Debris Clearance Robot for Extreme Environments,” in *Lecture Notes in Computer Science (including subseries Lecture Notes in Artificial Intelligence and Lecture Notes in Bioinformatics)*, vol. 11649 LNAI, pp. 148–159, Springer Verlag, jul 2019.
- [79] H. B. Wilson, L. H. Turcotte, and D. Halpern, “Third Edition Advanced Mathematics and Mechanics Applications Using,” tech. rep., 2003.
- [80] S. Soyulu, B. J. Buckham, and R. P. Podhorodeski, “Dynamics and control of tethered underwater-manipulator systems,” *MTS/IEEE Seattle, OCEANS 2010*, pp. 1–8, 2010.
- [81] C. Lambert, M. Nahon, B. Buckham, and M. Seto, “Dynamics and control of a towed underwater vehicle system, part I: Model development,” *Ocean Engineering*, 2003.
- [82] B. J. Buckham, *Dynamics modelling of low-tension tethers for submerged remotely operated vehicles*. PhD thesis, University of Victoria, 2003.
- [83] T. Ranganathan, V. Singh, R. Nair, and A. Thondiyath, “Design of a controllable variable buoyancy module and its performance analysis as a cascaded system for selective underwater deployment,” *Proc IMechE Part M: J Engineering for the Maritime Environment*, vol. 231, no. 4, pp. 888–901, 2017.
- [84] “Vortex Studio — Real-Time Simulation Software - CM Labs Simulations.”
- [85] “Vicon — Award Winning Motion Capture Systems.”

- [86] P. Merriaux, Y. Dupuis, R. Boutteau, P. Vasseur, and X. Savatier, “A study of vicon system positioning performance,” *Sensors (Switzerland)*, vol. 17, no. 7, pp. 1–18, 2017.
- [87] S. Tsai and T. Hahn, *Introduction to Composite Materials*, vol. 72. 2000.
- [88] Mflstrainingauges, “Long Strain Gauges - Strain Gauges.”
- [89] Omega, “Precision Strain Gages Extra-Long Grid Pattern for Inhomogeneous Materials.”
- [90] Cool Components, “Flex Sensor.”
- [91] “Error Analysis, Michigan State University.”